Structure, Energetics and Dynamics of Cs^+ and H_2O in Hectorite: Molecular Dynamics Simulations with an Unconstrained Substrate Surface

Narasimhan Loganathan[1], A. Ozgur Yazaydin[1,2], Geoffrey M. Bowers[3], Andrey G. Kalinichev[4] and R. James Kirkpatrick[5]*

[1] Department of Chemistry, Michigan State University, East Lansing, Michigan 48824, United States

[2] Department of Chemical Engineering, University College London, London, WC1E 7JE, United Kingdom

[3] Division of Chemistry, Alfred University, Alfred, New York 14802, United States

[4] Laboratoire SUBATECH (UMR-6457), Ecole des Mines de Nantes, F-44307, Nantes, France

[5] College of Natural Science, Michigan State University, East Lansing, Michigan 48824, United States

[*)] **Corresponding author e-mail:** naresh20@msu.edu

Telephone: (+1)517-353-1106

Abstract

Classical molecular dynamics (MD) simulations were performed for the smectite clay, hectorite, with charge balancing Cs^+ cations using a newly developed structural model with a disordered distribution of Li/Mg substitutions in the octahedral sheet and the fully flexible CLAYFF force field. Calculations for systems with interlayer galleries containing 0 to 19 H_2O/Cs^+ suggest that the mono-layer hydrate is the only stable state at all relative humidities at ambient pressure and temperature, in agreement with experimental results and previous molecular calculations. The basal spacing of this structure is also in good agreement with experimental values. In contrast to previous molecular modeling results, however, the new simulations show that interlayer Cs^+ occurs on 2 different inner sphere (IS) adsorption sites: above the center of ditrigonal cavities and above Si tetrahedra. Unlike previous simulations, which employed a rigid clay model and fixed orientations of the structural –OH groups, the present results are obtained for an unconstrained clay substrate structure, where the structural –OH groups are able to assume various orientations, including being nearly parallel to the clay layers. This flexibility allows the Cs^+ ions to approach the surface more closely above the centers of the hexagonal rings. In this structural arrangement, Cs^+ ions are not hydrated by the H_2O molecules which share the same interlayer plane, but rather by the H_2O molecules coordinated to the opposite surface. In contrast, on the external basal surface, a significant fraction of H_2O molecules are adsorbed above the centers of ditrigonal cavities adjacent to adsorbed Cs^+ ions. For these H_2O molecules, both H_{H2O} atoms coordinate and H-bond to O_b surface oxygen atoms. The mean residence times for the Cs^+ - H_2O, Cs^+ - O_b and H_2O - O_b coordination pairs show that Cs^+ ions are more strongly coordinated with O_b atoms than H_2O molecules. This result is the opposite of the behavior in Ca-hectorite, due to the much smaller hydration energy of Cs^+ compared to Ca^{2+}.

Introduction

Processes in clay mineral interlayer galleries and at mineral-water interfaces play a pivotal role in a wide variety of environmental and geochemical systems[1-5]. The adsorption of hydrated metal ions at mineral surfaces often controls their distribution in both natural and technological settings[6-10]. In particular, the very low permeability of natural clay-containing formations makes them potential host rocks for long-term geological disposal of toxic and radioactive waste,[11-15] CO_2 sequestration,[16-18] and control of reactive transport in the environment.[19-21] The sorption and transport properties of clays are strongly influenced by the following parameters: (i) the structure and composition of the clay mineral substrate;[22, 23] (ii) the composition and structure of the near-surface solution and its dynamics, which are different than in the bulk liquid phase;[23-26] and (iii) the structure of the nano-porous space connecting clay interlayers with inter-particle pores, including the pore size distribution. The transport properties and binding of mobile, hydrated species are different in the interlayer galleries and on external basal surfaces and edge sites than in bulk solution.[27,28] Molecular scale understanding of these differences is a prerequisite for developing quantitatively accurate transport models. Consequently, computational and experimental studies of the structure and mobility of H_2O and dissolved species at the surfaces and in the interlayers of clay minerals have increased greatly in recent years.[29-51]

Smectite clays are of particular importance because of their ability to intercalate cations and H_2O molecules in their interlayers and exchange these species with exterior pore solution. This exchange can cause interlayer expansion and bulk swelling that affects the macroscopic transport properties of fluids in clays.[36-38,44,47,50,52-58] The swelling energetics is strongly controlled by the clay composition, layer charge and cation hydration energy. For instance, the swelling of the smectite mineral hectorite and its interactions with metal ions and H_2O molecules have been

probed in detail using X-ray diffraction (XRD),[59-61] thermo-gravimetric analysis (TGA),[59,62,63] neutron scattering,[64-67] and NMR spectroscopy.[10,38,59,62,68-70] Interlayer structure and dynamics have been investigated by NMR[10,59,62,68-70] and neutron scattering studies.[64-67] Hectorite is widely used in NMR studies of smectites,[10,59,62,68,71] because its low Fe content minimizes paramagnetic effects on the probe nuclei. The results show that metal cations with higher hydration energies and smaller ionic radii are more prone to be hydrated and less often coordinated to the basal surface in inner sphere coordination than those with lower hydration energies and large ionic radii. The results clearly show that, irrespective of the metal cation, proximity-restricted H_2O molecules have structural and dynamical behavior different from that of the bulk solution. It is difficult, however, to experimentally distinguish H_2O molecules and cations in the interlayer galleries from those on external surfaces and to separately characterize their structural and dynamical behavior.

Computational molecular modeling studies are providing invaluable atomistic information about the underlying physico-chemical properties of smectite-water-cation systems and deeper, molecular scale interpretation of the experimental data. For instance, the intercalation of organic compounds and inorganic metal cations into hydroxy/fluoro-hectorites has been examined in detail using molecular simulations.[57,65,70,72-76] For hydroxyl-hectorite, Morrow et al.[73] showed that Na^+ ions are adsorbed as outer sphere surface complexes, except at low H_2O contents. Recent modeling of Na^+ and H_2O sorption on the surfaces of inter-particle hectorite nano-pores by Greathouse et al.[74] has shown that the structure of the siloxane surface of the clay affects the H_2O adsorption.

Adsorption and transport of Cs^+ in clay materials is of particular interest, because Cs^+ is a principal component of many radioactive wastes, has high aqueous solubility, and is not subject to solubility-limiting precipitation.[10,62,77] Recent studies have focused on the adsorption of Cs^+ in clay minerals following the substantial discharge of ^{137}Cs in the aftermath of the Fukushima

incident.[78,79] After accidental release, the retention of Cs^+ near and just below the earth's surface is controlled primarily by its sorption in soils, in which clay minerals are important constituents. The sorption characteristics of Cs^+ varies greatly between different mineral surfaces. Experimental studies have reported that it adsorbs in inner sphere coordination at the relatively highly charged muscovite surface,[32] whereas EXAFS studies using the lower charge montmorillonite suggest outer sphere complexation.[80-82] In addition, Cs^+ also has the smallest charge/ionic radius ratio and the smallest hydration energy of all of the group I and II elements, making it an important end member case for understanding the behavior of smectites with a wide range of other exchangeable cations. Simulations by Sutton and Sposito[75,76] suggested that Cs^+ is adsorbed in inner sphere coordination in the interlayers of hydroxyl-hectorite and other smectites at all hydration states. Recent experiments and associated simulations by Porion et al.[70] indicate that at 97% relative humidity (RH), the interlayer water content of synthetic Cs-fluorohectorites with a basal spacing of 12.2 Å, corresponding to a mono-layer hydrate, is 4.2 H_2O molecules per Cs^+. Although these results provide new insight into the behavior of Cs^+ and water molecules in hydrated interlayer galleries, the specific structural environments of these species and the differences in the structural arrangements, H_2O orientation, and the dynamics of Cs^+ and H_2O molecules in the interlayer galleries and on the external basal surfaces remain incompletely understood.

The main objectives of the current study are to fill this gap by developing larger and more realistic hectorite models with disordered distributions of Li^+ for Mg^{2+} substitution in the octahedral sheet and to use these models to more deeply examine the structure, dynamics and swelling energetics of Cs-hectorite. We observe significant differences in the adsorption sites for Cs^+ and the orientation of H_2O molecules when compared to earlier studies.[75,76] These differences suggest that the adsorption structure and dynamics is strongly correlated with the reorientation of

OH^- groups in the octahedral layer of the clay. Potentially stable hydration states are determined based on calculated thermodynamic parameters related to swelling, and the molecular-scale structure and dynamics of the potentially stable hydration states are evaluated. The relationships between the structures of the surface adsorption sites, the orientation of the interfacial water molecules, their participation in the hydrogen bonding network, and the Cs^+/H_2O ratios for both clay interlayer and external hectorite surface are characterized in detail. The simulation results are in good agreement with available experimental NMR and XRD measurements.[10, 62, 70, 83, 84]

Simulation Details

Hectorite is a 2:1 trioctahedral smectitic clay mineral that develops permanent, negative structural charge by Li^+ for Mg^{2+} substitution in the octahedral layer. Our model has the structural formula of $M^+(Mg_5Li)Si_8O_{20}(OH)_4$. The structure is composed of two sheets of SiO_4 tetrahedra sandwiching a sheet of $Mg,Li(OH)_2$ octahedra. The net negative structural charge is compensated by interlayer cations. The model hectorite structure used in our simulations is based on that of Breu et al.[85] The Li^+/Mg^{2+} ratio of 1/5 is similar to the composition of natural San Bernardino hectorite used in our experimental studies,[10,38,59,62,68,71] although the natural sample contains both OH^- and F^-. The hydration of fluoro-hectorite has been previously investigated.[65,67,86] The natural sample also has a very small fraction (0.25%) of tetrahedral Al^{3+}/Si^{4+} substitution that is not incorporated into the simulations.

For studies of the interlayer galleries, the simulation supercell contains 2 interlayers and consists of 40 unit cells of hectorite (5×4×2) with lateral dimensions of approximately $L_x \approx 26$ Å and $L_y \approx 36$ Å. This size allows for a disordered distribution of the substitution sites and corresponding structural charge (Figure 1a). This distribution was developed by replicating the

unit cell of hectorite in all crystallographic directions to fill the simulation supercell before isomorphic substitutions were assigned. This procedure yields a simulation supercell in which each TOT layer has a different arrangement of Li^+ in the octahedral sheet. Substitutions were performed ensuring that there is no aggregation of structural charge around a substituted octahedral site, thereby eliminating charge gradients in the system. All interlayer Na^+ in the constructed model were replaced by Cs^+, which were initially placed at the mid-plane of the interlayers. In order to understand the effects of interlayer hydration, the models were prepared using 25 different hydration levels with the water contents ranging from 0 to 20 H_2O molecules per Cs^+ ion. The initial *c* dimensions of the models were slightly larger than the expected final value to allow for better equilibration. Since the clay layer charge in our system is -1.0|*e*| per crystallographic unit cell, the quantitative measure of water content expressed as H_2O/Cs^+ or H_2O/(unit cell) in our case is numerically the same.

The external hectorite surface was constructed by cleaving the structure along the (001) plane at the middle of the interlayer space. After cleavage, one-half of the interlayer Na^+ ions were retained at their initial positions on the basal (001) surface and replaced by Cs^+. As for the interlayer simulations, the simulation cell consists of 3 hectorite layers with a thickness of ~29 Å. In the final simulation supercell, these surfaces were separated by ~144 Å along the *z* direction to simulate a nano-pore. Both lateral dimensions were ~72 Å. The large nano-pore thickness perpendicular to the surface eliminates any direct interaction of one surface with the other when the periodic boundary conditions are applied. As for the interlayer simulations, all the octahedral Li^+/Mg^{2+} substitutions were distributed in a disordered manner. All the Cs^+ were initially placed 15 Å from the hectorite surface to allow them to choose their preferred adsorption sites during the course of the simulation. The interlayers contained no H_2O to save computation time. Initially,

two separate H_2O slabs each with a thickness of 50 Å were placed on the two hectorite (001) surfaces with ~15 Å vapor phase at the middle of the nano-pore. This water film is sufficiently thick to characterize both the interfacial features of the structure and the bulk-water behavior in the nano-pores, as demonstrated in previous simulation studies.[39,42,58]

Molecular Dynamics (MD) simulations using the statistical *NPT* (constant *N* number of atoms, constant pressure *P* and constant Temperature *T*) and *NVT* (constant *N* number of atoms, constant volume *V* and constant Temperature *T*) ensembles were performed using the LAMMPS simulation code.[87] A Nosé-Hoover thermostat and barostat were used to control the temperature and the pressure independently in all 3 dimensions.[88,89] Three-dimensional periodic boundary conditions were employed, and the interatomic interactions for all species were calculated using the CLAYFF[90] force field that is well tested in molecular simulations of clays and related materials.[73,74,91,92] The flexible SPC water model was used to describe the interactions of H_2O molecules with the clay structure and hydrated ions.[93] *NPT* simulations were first carried out for each hydration level at ambient conditions (P = 1 bar and T = 300 K). A cutoff distance of 10 Å was applied for the short range non-electrostatic interactions, and Ewald summation technique was used to calculate long range electrostatic interactions. A time step of 1 fs was employed to integrate the equations of atomic motion, and each system was equilibrated for 2 ns before a data production run of another 2 ns was started. The MD trajectory was recorded every 10 fs over the last 2 ns of the *NPT* production run. In these simulations the cell dimensions were allowed to vary independently and change with water content. The cell dimensions and thermodynamic quantities (e.g., basal spacing, hydration and immersion energies, and isosteric heats of adsorption) were calculated for every hydration state. These quantities were computed using 10 equal, statistically independent time blocks, yielding small standard errors for the reported averages. Potentially

stable hydration states were determined by analyzing the data from the *NPT* simulations. *NVT* simulations for these stable hydration states were performed for another 4 ns, which includes 2 ns of additional equilibration followed by 2 ns of data production. The initial configurations for the *NVT* simulations were the average atomic positions during the last 2 ns of the *NPT* production run. The *NVT* simulations of the external basal surface were performed in a similar manner after initial equilibration under ambient conditions for 6 ns. The data from the last 2 ns trajectory of the *NVT* simulation runs were recorded every 10 fs were used to determine the structure and dynamics of the water molecules and exchangeable cations for both the interlayer and external surface simulations.

The swelling energetics were evaluated using the hydration and immersion energies and the isosteric heats of adsorption, The hydration energy is the energy change that occurs when water is added to the dry clay and is given by

$$\Delta U = \frac{\langle U(N)\rangle - \langle U(0)\rangle}{N} \quad (1)$$

where N is the number of interlayer water molecules adsorbed on the clay, and $\langle U(N)\rangle$ and $\langle U(0)\rangle$ are the average potential energies of the equilibrated hydrated and dry clays, respectively.[23,94] The immersion energy, Q is the energy released or gained when the clay hydration is increased from one level to another by adding water to the system and is given by

$$Q = \langle U(N)\rangle - \langle U(N_{\mathrm{ref}})\rangle - (N - N_{\mathrm{ref}})U_{\mathrm{bulk}} \quad (2)$$

where N_{ref} and $\langle U(N_{\mathrm{ref}})\rangle$ are the number of interlayer water molecules and the average potential energy of a reference hydration state. Here we use the system with the highest water content as the reference hydration level, because its value is closer to that of bulk water than any of the other simulations. The isosteric heat of adsorption is the enthalpy change of a system per mole of water when an infinitesimal amount of water is added to an existing water content[50,54,94] and is given by

$$q_{st} = RT - \frac{\langle U(N)\rangle - \langle U(N')\rangle}{(N'-N)} \quad (3)$$

where N and N' are number of water molecules in two consecutive hydration levels, R is the ideal gas constant, T indicates temperature, and the term RT is used to convert energy and enthalpy for the vaporization process. Stable hydration states are represented by the water contents at which the computed relationship crosses the bulk vaporization enthalpy of SPC water (-44 kJ/mol) with negative slope. Although all three of these quantities are based on the same computed thermodynamic information, they are related to different experimental techniques. The immersion energies yield a clear representation of the hydration states and can be directly compared with calorimetric measurements.

The structural properties of the hydrated interlayers and external surfaces were quantified by calculating the atomic density distributions of all species both perpendicular and parallel to the hectorite surface. The widths and positions of each peak of the atomic density profiles perpendicular to the surface were used to define the limits for the analysis of the atomic densities for structurally different types of atoms within planar volumes parallel to the surface. The orientations of H_2O molecules with respect to the hectorite surface were evaluated using the angles that the molecular dipoles and H-H vectors make with respect to the surface normal. Though other H-bond definitions are possible,[95,96] the H-bonding networks reported here both within the interlayer galleries and at the external basal surface were analyzed by applying a commonly used geometric criteria of an H-bond. In this definition, a hydrogen bond is assumed to exist if and only if the intermolecular O···H distance is less than 2.45 Å and the angle between the O···O and O-H vectors is less than 30º.[23,39,42] For the purpose of H-bonding calculations, the oxygen atoms of the basal clay surface (O_b) were treated in the same way as O_{H2O} (i.e., as potential H-bond acceptors). The origin for analysis of the atomic density profiles was the mean position of the surface O_b

atoms. In the structures of the mono-, bi- and tri-layer hydrates these profiles were calculated by averaging over two statistically independent interlayer regions, each with the same number of water molecules. H_2O diffusion coefficients were calculated from all simulations using mean-square displacements,[39,42,50,73] but diffusion along *z* direction is limited in the interlayer. Diffusion coefficients of the cations are correlated with the distribution and orientation of H_2O molecules near the hectorite surface.

The dynamical behavior of the H_2O molecules were quantified through the characteristic time they spend in coordination with the O_b atoms, in the first hydration shell of Cs^+, and in coordination with other H_2O molecules. The average residence times of H_2O molecules in different coordinations were determined using time autocorrelation functions in a way similar to those employed in the description of hydrogen bond lifetimes.[97,98] Two different mean residence times are reported here based on the population analysis and are termed the intermittent $c(t)$ and continuous $C(t)$ time correlation functions. For the intermittent correlation function, $c(t) = 1$ when an H_2O molecule is present in the first coordination shell of a metal ion or an O_b at time $t=0$ and at a later time t. Otherwise $c(t) = 0$. For this function, an individual H_2O molecule can leave the coordination shell and still be considered coordinated ($c(t)=1$) if it re-enters the same coordination shell during the time period considered. For the continuous correlation function, $C(t) = 1$ when an H_2O molecule is present in the first coordination shell of a metal ion or O_b at time $t=0$ and remains in the same coordination continuously thereafter until the end of the simulation. Otherwise $C(t) = 0$. Re-entries do not cause $C(t)$ to become 1 again. A time interval of 2 ps was used for computing these averages. This period is comparable to the residence times of H_2O molecules in cation hydration shells, as determined in earlier studies.[99-101] The methods of analysis used here have been previously described in detail.[39,42,50,73]

Results and Discussion

Thermodynamic quantities

The interlayer spacing of Cs-hectorite increases continuously with increasing water content, with a somewhat smaller slope between 1 and 4 H_2O/Cs^+ as water molecules fill the spaces between Cs^+ ions (Figure 2a). The computed interlayer spacing of the completely dehydrated hectorite is 10.75 Å, in good agreement with the experimental value of 10.65 ± 0.2 Å obtained using X-ray diffraction techniques (Table 1).[83,102] It is also consistent with the values for other dry Cs-smectites such as Cs-montmorillonite.[50,94,103] It is significantly greater than the computed value for dry Na-hectorite[73] due to the larger ionic radius of Cs^+ (~1.7 Å vs ~1.0 Å). With increasing hydration, a stable monolayer hydrate is represented by the plateau at ~12.4 Å. This value is also in good agreement with the values of 12.2-12.5 Å obtained in previous molecular simulations and experimental studies of Cs-hectorite.[70,75,76,83,84,104] This stable monolayer hydrate has 4 H_2O/Cs^+, also consistent with previous simulation and experimental studies,[70] although some of the experimental values are for synthetic fluoro-hectorites.[70] The similarity between the experimental and computed values suggests that the basal spacings are not greatly affected by OH^-/F^- substitution, assuming the same interlayer water content. Further increase in hydration results in a linear increase in the computed interlayer spacing of Cs-hectorite.

Previous experimental and simulation studies have shown that smectite minerals can have stable structures with up to 4 water layers depending on the nature of the charge-balancing cation and structure and composition of the clay.[50,55,94,103] For Cs-hectorite, however, the available experimental data show only the mono-layer hydrate at all externally imposed water activities at ambient temperature and pressure.[70,84] The computed hydration energies[50,73] for Cs-hectorite

(Figure 2b) show a well-defined energy minimum (-50 kJ/mol) at $H_2O/Cs^+ = 4$. The location and depth of this minimum are consistent with our basal spacing calculations and previous simulation results[70,75,76] for the mono-layer hydrate. The quantitative energy differences (~4 kJ/mol) between the computed hydration energies here and in previous studies of Cs-hectorite are probably due to the different interaction models (SPC *vs* MCY) employed in the simulations.[75,76] The hydration energies also shows two shallower minima at $H_2O/Cs^+ = 9$ and 14.5 with values of -44.5 and -43 kJ/mol, respectively, but there are no corresponding plateaus in the computed basal spacings (Figure 2a). These two states represent bi- and tri-layer hydrate structures. The values of the minima are only a few kJ/mol less than value of the internal energy of bulk SPC water (-41.2 kJ/mol), suggesting that mono-layer structure is stable and the others are not. This conclusion is in good agreement with the experimental studies, and the bi- and tri-layer hydrates should be considered as hypothetical. As the water content increases, the hydration energy approaches the value for bulk SPC water.

The calculated immersion energies (Eq. 2; Figure 2c) help better define the positions of the bi- and tri-layer hydrates and corroborate the H_2O/Cs^+ ratios of the hydration states at 4, 9 and 14.5. Even though stable hydration states with more than one water layer are not observed experimentally under ambient conditions, analysis of the higher hydrates yields useful structural, dynamical and energetic information about such experimentally inaccessible hypothetical structures, thus helping to understand the underlying molecular origins of the observed behavior of the modeled material and other comparable phases,[50,91] including hectorite with other exchangeable cations. The computed isosteric heats of adsorption (Figure 2d) also clearly show the three hydration states. The overall conclusions for Cs-hectorite are comparable to those for Cs-montmorillonite, for which only the mono-layer structure is observed experimentally, [84,104,105] but

for which hypothetical higher hydration states were also simulated.[50,54,55,94,103] The H_2O/Cs^+ ratios in hectorite are always less than for Cs-montmorillonite for all 3 hydration states. This could be due to the inherent structural differences (trioctahedral *vs* dioctahedral T-O-T layers) between hectorite and montmorillonite or due to the presence of both tetrahedral (Al^{3+} for Si^{4+}) and octahedral (Mg^{2+} for Al^{3+}) substitution in the modeled montmorillonites (see, e.g., refs. 50, 54). Nevertheless, the H_2O/Cs^+ ratios for different hydration states in our study are consistent with the range reported for Cs-montmorillonite simulated using only octahedral substitutions.[103]

Atomic density profiles

The atomic density profiles (ADPs) of Cs^+ ions and H_2O molecules as a function of distance from the hectorite surface for external surfaces and for interlayer galleries with 1, 2 and 3 water layers, as defined by the minima in the hydration energies, show similar patterns with Cs^+ occupying predominantly two types of inner sphere sites (Figure 3).

For the monolayer hydrate (Figure 3a), the Cs^+ ions located at distances of approximately 2.1 Å and 3.9 Å from the reference basal surface (z = 0 Å) are on the same types of adsorption sites but are coordinated to the left (~0 Å) and right (~6 Å) hectorite surfaces, respectively. The Cs^+ peak at 3.0 Å is at the center of the interlayer. Based solely on the ionic radii of Cs^+ (1.9Å) and O_b (1.5Å) it is clear that the Cs^+ ions at 2.1 Å and 3.9 Å are in inner sphere coordination with respect to one of the basal surfaces and that the one at 3.0 Å is inner sphere coordination with respect to both surfaces. The O_{H2O} ADP of the monolayer hydrate consists of 2 peaks of equal intensity located at 2.6Å and 3.4Å. These two peaks represent layers of H_2O molecules that are not far enough apart along the z direction to be separated by Cs^+ ions. The corresponding H_{H2O} peaks are centered at 1.6, 3.0 and 4.4 Å. Since the integral intensities of O_{H2O} at 2.6 and 3.4 Å and

the H_{H2O} peaks at 1.6 and 4.4 Å are similar and the distance between them is approximately 1.0 Å (i.e., comparable with the length of the intramolecular O-H bond of H_2O molecules), we can conclude that these water molecules are oriented in a manner that, at least in principal, allows them to donate one H-bond to the O_b. Evaluation of H-bond donation to other water molecules by the H-atoms in the mid-plane peak at 3 Å requires additional information and is discussed below.

The O_{H2O} distribution with two maxima for the monolayer hydrate of Cs-hectorite contrasts with that of the monolayer hydrate of Na-hectorite, which has one maximum at the mid-plane of the interlayer.[73] This is due to the fact that all the Na^+ ions lie in the middle of the interlayers, and to hydrate them the H_2O molecules are arranged in the same plane. In contrast, in our simulations of Cs-hectorite, the Cs^+ ions are equally distributed between the two basal surfaces leading to two H_2O sub-layers for this hydration state.

Although the computed interlayer spacings for our monolayer Cs-hectorite and those from the previous work[75,76] are similar, the Cs^+ ADPs are significantly different. The previous simulations suggest that at this hydration state Cs^+ occurs on one type of site, is located at the mid-plane of the interlayer gallery at the same level as the O_{H2O}, and has a coordination number of 6.0 with respect to both basal surfaces. In contrast, our results suggest that Cs^+ occurs on two types of sites at different distances from the basal surfaces, consistent with ^{133}Cs NMR results.[10,62] These NMR spectra for samples equilibrated at 100% RH and mixed with water to form a paste show the presence of two Cs sites. We assign the NMR peak at -29 ppm to the Cs^+ ions closest to the basal surfaces and one with less negative or more positive chemical shifts to the Cs^+ ion further from the surface.[10,62]

The differences between our results and those from previous simulations are most probably due to the differences in the force fields used in the simulations. Compared to our model, Sutton and Sposito[75,76] used a hecorite unit cell with a slightly lower total structural charge (-0.8|*e*| *vs* -1.0|*e*|) and the Skipper-Smith force field parameterization[94,106] that assigns full formal charges to the atoms in the octahedral layer (q_{Mg} =+2.0|*e*|; q_{Li} = +1.0|*e*|). In contrast, the CLAYFF parameterisation used here[90] assigns partial charges (q_{Mg} =+1.36|*e*|; q_{Li} = +0.525|*e*|). In addition, in the Skipper-Smith model the charges on the hydroxyl O atoms are much more negative than in CLAYFF (-1.42|*e*| *vs* -0.95|*e*|), while the apical O atoms (-1.31|*e*| around Li and -1.28|*e*| around Mg) in CLAYFF have slightly higher negative charge than in the Skipper-Smith model which uses -1.0|*e*| for all O atoms around Mg or Li octahedra. Thus, on balance, the electrostatic repulsion between the octahedral cations and the surface Cs^+ ions is expected to be higher in their simulations than in our's. Another important difference is that the Skipper-Smith model[94,106] used by Sutton and Sposito[75,76] assumes a rigid structure for the T-O-T clay layers in which the structural –OH groups are all constrained to be oriented perpendicular to the layers. In contrast, our simulations allowed all atoms of the hectorite structure to move according to the interaction parameters described by the CLAYFF force field,[90] resulting in fully flexible T-O-T clay layers. The most important outcome of this is that in our simulations the structural –OH groups are reoriented to angles up to 90º with respect to the normal to the hectorite layers, rather than always staying perpendicular to them. Together, these differences allow Cs^+ ion in our simulations to find adsorption sites closer to the surface. In our structures, the –OH groups that are part of Li-substituted octahedral sites can be oriented both parallel and perpendicular to the surface, whereas almost all of them that are part of non-substituted Mg-octahedra are usually at high angles between 60º and 90º to the surface normal.

The ADPs for the hypothetical bi- and tri- layer hectorite hydrates are similar to that of the monolayer structure in the near surface region (Figures 3b and 3c). These similarities are in agreement with the general notion that Cs^+ prefers coordination by O_b atoms to being hydrated by water molecules. The Cs^+ density distributions in the bi- and tri-layer hydrates both have 2 peaks at 2.1 and 3.0 Å, comparable to the two peaks observed for the monolayer hydrate. There is also a small, broad distribution of Cs^+ atomic density in the central part of the interlayer at distances greater than 4.0 Å from the surface. The latter represents Cs^+ ions that move between the basal surfaces and form outer sphere surface complexes, as they do in other smectites.[50,76] The ADPs of O_{H2O} and H_{H2O} are also similar for the different hydrates. O_{H2O} has maxima at 2.6 and 3.6 Å, positions similar to the two maxima in the monolayer hydrate. H_{H2O} has maxima at 1.6 and 3.0 Å, again similar to the positions for the monolayer hydrate. The structural interpretation for these peaks is the same for all hydration states. The mid-plane regions of the bi- and tri-layer hydrates are quite different, with broad peaks for O_{H2O} and H_{H2O} for the 3 layer hydrate due to the need to fill the interlayer space.

The interlayer ADP's for Cs^+ ions and H_2O molecules for all hydration states are in reasonable agreement with modeling studies of Cs-montmorillonite[50] using the CLAYFF[90] force field, but differ from the previous simulation studies of Cs-montmorillonite[75,76,94,103,107] for monolayer hydrate using the Skipper-Smith force field[94,106] (see the discussion above). However, as the hydration state increases, Cs^+ ions in those previous simulations[103,107] are shown to predominantly adsorb closer to the substrate surface. This result is qualitatively consistent with present study. In contrast, the first H_2O molecular layer is adsorbed at similar distances with H_{H2O} atoms lying closer to the substrate surface in accordance with our results.[94,103,107]

The ADPs of Cs^+ and H_2O in the near-surface (~4 Å) region of the external surfaces are essentially identical to their distributions in interlayers of the bi- and tri-layer hydrates, except for a shoulder for O_{H2O} at approximately 2.2 Å, which we discuss below (Figure 3d). Further from the surface, Cs^+ atomic density exhibits a peak at 5.3 Å, and O_{H2O} and H_{H2O} show several broad features up to 10 Å. Beyond this distance both O_{H2O} and H_{H2O} distributions show bulk-like water behavior. These results are in reasonable agreement with previous simulation studies of external surfaces of Cs-montmorillonite, which show Cs^+ in both inner and outer sphere coordination.[108,109] However, these studies[108,109] suggest that inner sphere Cs^+ adsorption occurs dominantly above Si tetrahedra, in contrast to our results, which indicate Cs^+ adsorption (~65%) above the center of ditrigonal cavities is dominant. In addition, the proximity-restricted H_2O molecules in previous studies coordinate and form H-bonds with the surface only through one of their H_{H2O} atoms, whereas in our simulations, ~25% of the surface ditrigonal cavities have H_2O molecules coordinating through two H-bonds, as we discuss below in detail.

Angular distributions: the orientation of the water molecules

The orientation of H_2O molecules in the interlayer galleries of smectite minerals plays an important role in determining the basal spacings and is critical to the formation of stable H-bonding networks. We characterize the H_2O orientations using the angles between the calculated dipole and HH vectors and the normal to the clay surface for both the interlayer and external basal surface. The probability density distribution of the angle between the surface normal and the H_2O dipole vector as a function of distance from the basal surface (Figure 4a) clearly shows that for the experimentally stable monolayer hydrate, the near surface adsorbed H_2O molecules (z ~ 2-3 Å and 3-4 Å) have their dipole vectors oriented towards the left (100º-140º) and right (35º-80º) hectorite surfaces in Figure 3, respectively. The average angle between the H_2O dipole and the surface

normal is 60.75°. However, the dipole vectors of a small fraction (~2%) of H_2O molecules at distances $z < 2$ Å or $z > 4$ Å are oriented perpendicular to the corresponding hectorite surfaces (Figure 4a). Nevertheless, the absence of HH vectors parallel to the hectorite surface for H_2O molecules at these distances (Figure 4b) show that orientations with the dipole vector perpendicular to the hectorite surface are statistically unlikely. This conclusion is consistent with the ADPs of the monolayer hydrate, which indicate that the H_2O molecules are principally arranged with only one H_{H2O} pointing towards the surface. This result is quite different than in previous studies of Cs-hectorite.[75,76] For instance, these earlier studies proposed that irrespective of the water content, the dipole vectors exhibit two orientations, parallel and perpendicular to the basal surface, with the perpendicular orientation dominating at high water content. In our simulations, H_2O molecules at distances $z < 3$ Å have their dipoles pointed towards the hectorite surface at all hydration states. As for the differences in the ADPs discussed above, these differences are probably caused by a combination of the differences in the clay structural charge, interaction potentials,[94,106] and the flexibility of the clay structure. Earlier simulation studies of Cs-montmorillonite with only octahedral substitutions have clearly indicated that the near surface adsorbed H_2O molecules have their dipoles oriented towards the smectite surface, consistent with current study.[103,107]

The orientations of the H_2O molecules in the near surface region ($z < 10.0$ Å) of the external Cs-hectorite basal surface in our simulations are very similar to those in the interlayer galleries except at distances $z < 2.0$ Å (Figures 4c and 4d). The dipole vectors of H_2O molecules at these distances are parallel to the surface normal and the HH vectors are perpendicular to it. This result is in disagreement with the calculations of Sutton and Sposito,[75,76] which locate the O_{H2O} atoms closer to the surface than the H-atoms. Again, we believe that this is the result of the different

structural charge, different interaction potentials,[106] and substrate flexibility, which allows the structural –OH groups in our simulations to reorient. In the Sutton and Sposito simulations,[75,76] the near surface electrostatic attraction between the H_{OH} and the O_{H2O} is greater than when the H_{OH} can relax to their expected non-perpendicular configurations, as in our calculations. With increasing distance from the surface, the H_2O molecules in our simulations are arranged with their dipoles oriented towards and away from the hectorite surface, consistent with previous studies of the surface of Cs-muscovite mica and Cs-montmorillonite.[32,39,108] The H-bond structure in our simulations is consistent with these interpretations and is discussed in detail in the Supplementary Materials.

Radial distribution functions

The radial distribution functions (RDFs) and running coordination number (RCNs) for Cs^+ - O_{H2O} and Cs^+ - O_b pairs in the interlayer region for mono-, bi- and tri-layer hydrate and on the external basal surface (Figures 5a and 5b) show that irrespective of the hydration level the mean interatomic distances between Cs^+ - O_{H2O} and Cs^+ - O_b pairs are centered at 3.1 Å and 3.3 Å, respectively. These values are very similar to the Cs^+-H_2O distances in bulk solution[111,112] and in previous simulations studies of smectite surfaces.[103,108] The hydration structure reported for montmorillonite using experimental EXAFS methods indicates average Cs - O distances of 3.0 – 3.2 Å and 3.6 - 4.2 Å for 1st and 2nd coordination shell respectively.[80,81] However, Bostick et al.[80] and Fan et al.[81] claim that the Cs^+ ions with the shorter Cs - O distances, which have RCNs of 3-5, are present in outer sphere surface complexes, completely hydrated and hence separated from surface through H_2O molecules. They also propose that the Cs^+ ions with larger Cs – O distances are in partially dehydrated inner sphere complexes. However, our simulations results indicate that the Cs^+-O_b distances are slightly greater than the Cs^+-O_{H2O} distances, and do not support these

conclusions. Instead, our results clearly indicate that the majority of the Cs^+ ions are adsorbed on inner sphere sites coordinated to 4-6 surface O_b atoms. The Cs^+-O_b RCN decreases with increasing hydration state, but Cs^+ still prefers to be in inner sphere coordination, as also observed in previous simulation studies using montmorillonite.[103] It is worth noting that EXAFS measurements cannot distinguish between O_b and O_{H2O} atoms around Cs,[82] and this can probably explain the above disagreements in interpretation of the surface structure.

The RCNs in our simulations of the monolayer hydrate are, however, quite different from those of the other hydration states and the external surface. For the monolayer hydrate, the nearest neighbor coordination of Cs^+ is 6.4 O_b and 4.2 O_{H2O} for total of 10.5. As the interlayer hydration level increases, Cs^+ is coordinated by progressively fewer O_b and more O_{H2O}, but the total average coordination remains in the range of 10.2-10.5. These results are in reasonable agreement with previous simulation studies for the interlayers of Cs-hectorite and other Cs-smectites.[50,54,75,76] The RDF and RCN of both pairs on the external surfaces are similar to the distributions for the bi- and tri-layer hydrates, although the RCN of O_b coordination is even less. The total coordination of the surface Cs^+ ions is 10.1 with 3.3 O_b and 6.8 O_{H2O}. These values are in good agreement with previous simulations at higher hydration levels[75,76] in the interlayer region. Again, the differences in the RCNs in our simulations and in earlier simulations are probably due to differences in the substrate surface charge, the clay structure, the interaction potentials used, and the substrate flexibility used in our models.[50,103,107-109]

Planar atomic density distributions

Planar atomic density distributions (PADDs; also known as atomic density maps) provide more detailed information about the structural environments of the water molecules and

exchangeable cations in the interlayers and external surfaces. For Cs-hectorite they show that in the interlayers and on the external surfaces Cs^+ ions are adsorbed on two types of sites with different coordinations to the O_b, as expected from the ADP's (Figures 6a-6d). The Cs^+ ions located closest to the surface (atomic density maximum at ~2.1 Å) are adsorbed at the centers of ditrigonal cavities and are highly localized (Figure 6a). In contrast, those located ~3.0 Å from the surface are adsorbed above the Si tetrahedra and are much more mobile (Figure 6a). In the monolayer hydrate, the Cs^+ ions located above the center of the ditrigonal cavities are coordinated by 6.0 O_b, while the coordinating water molecules are themselves adsorbed on the opposite interlayer surface (Figure 6b). Thus, the PADDs of O_{H2O} coordinating Cs^+ shown in Figure 6a are not located in the same plane as the Cs^+ ($z \leq 2.5$ Å) but at $z > 3$ Å with their H_{H2O} pointing towards and away from the hectorite surface at $z = 6$ Å (see Figures S2 and S3 in the Supporting Information). The dense O_{H2O} contours clearly reveal that the H_2O molecules hydrating the hectorite surface are responsible for the hydration of Cs^+ ions that are adsorbed at the opposite surface. To our knowledge, no previous simulation studies have reported similar interlayer structures. In contrast, the Cs^+ ions at $z = 3$ Å are partially hydrated by both H_2O molecular layers and are dispersed over the interlayer surface.

The Cs^+ ions at $z < 2.5$ Å (center of ditrigonal cavities) in the monolayer hydrate are not adsorbed uniformly within the plane of the interlayer, but are concentrated in regions with lateral dimensions of approximately 20 Å × 17 Å. The other regions are occupied by H_2O molecules, which share approximately the same plane. The long range ordering of the Cs^+ ions and H_2O molecules is similar to their arrangements in previous simulations using mica.[110] Such arrangements occur because they allow H_2O molecules to form more and stronger H-bonds among themselves than they would otherwise have. Two important points support the computed structural

arrangement. (i) The absence of significant charge inhomogeneities in the modeled hectorite structures rules out their impact on the interlayer structure, since the charge is homogenously distributed over entire surface, but without any repetitive Li^+/Mg^{2+} pattern. (ii) In additional simulations with high initial temperatures (700 K) that were gradually reduced to 300 K the final arrangement of Cs^+ ion and H_2O molecules was essentially identical to that in the original simulations. The initial high temperature provides greater atomic mobility and reduces the possibility of artifacts in the final computed models. However, the Cs^+ ions located ~3 Å from the surface (center of interlayer) are dispersed over the entire hectorite surface which suggests that they oscillate between lower and upper hectorite surfaces of the interlayer and are mobile when compared to Cs^+ ions located at the center of ditrigonal cavities.

The computed model of the bilayer hydrate also shows significant long range ordering of Cs^+, the PADDs show that the H_2O molecules contributing to the O_{H2O} ADP peak at 2.6 Å (sharing same plane as Cs^+) are responsible for the hydration of both a hectorite surface and metal ions belonging to that surface (See Figure 6c). Figure S4 (see Supporting Information) indicates a strong ordering of H_{H2O} contours pointing towards the O_b atoms, and the H_{H2O} contours in Figure S5 (Supporting Information) show a dispersed structure. This structure indicates that the H_2O molecules are arranged with one hydrogen pointed towards a surface, with the other is responsible for H-bond interactions with other H_2O molecules at the same plane or at larger distances from the surface.

In the discussion above, we claim that the H_2O molecules on the external (basal) surface show characteristics similar to the hypothetical bi- and tri-layer hydrates, except at distances $z <$ 2 Å. These H_2O molecules are in the shoulder region in the ADP (Figure 3d). The PADD in Figure 6d confirms that they are adsorbed at the centers of ditrigonal cavities with their H_{H2O} pointing

towards the surface and that they exhibit symmetric, rotationally averaged contours. This structure is consistent with the results from the H_2O orientation and H-bond distribution calculations. This is also in reasonable agreement with previous simulations with higher charge mica substrates.[23,39,110] Because of the relatively small structural charge of hectorite, only a fraction of the ditrigonal cavities are occupied by H_2O molecules. This is in contrast to the muscovite surface, where ~50% of the cavities are occupied due to the high structural charge due to isomorphic substitution in the tetrahedral layer. The PADD of the water molecules contributing to the peak at 2.7 Å of the O_{H2O} ADP (Figure S6 of Supporting Information) shows a distribution similar to the ones for interlayer H_2O molecules in the bi- and tri-layer hydrates. Previous simulation studies of Cs-montmorillonite have suggested a similar adsorption structure for the first adsorbed H_2O molecular layer.[107,108] However, in contrast to our studies, in which the O_{H2O} distributions overlap the distribution of H_{H2O} atoms pointing towards the surface O_b atoms, the earlier studies showed O_{H2O} atoms offset from the H_{H2O} atoms and located slightly towards the ditrigonal cavities. As for the other differences between the earlier results and ours, this difference is probably due to a combination of the different clay structural charges, clay structures, interaction potentials[106] and flexibility of the clay substrate. Overall, it is evident in our results that at all water contents, the maxima of the H_{H2O} distributions (but not those of O_{H2O}) are closer to the hectorite surface, than it was concluded from the previous studies.[75,76] These results clearly indicate how the simulation methods and interatomic potentials can affect the water arrangement in the interlayer galleries and on external surfaces.

Water diffusion

Many computational MD studies have reported that the H_2O diffusion coefficients in interlayer galleries are significantly lower than in bulk solution or on the external surfaces and that

they increase with increasing the interlayer water content.[43,50,54,73,75,76,103,113,114] The diffusion coefficients from our simulations (Table 2) are in generally good agreement with previous simulations.[43,50,54,73,75,76] However, the diffusion coefficient reported here for the monolayer hydrate is a factor of four smaller than in previous simulations of hectorite.[75,76] This difference is probably due to the interlayer H_2O molecules being split into two sublayers hydrating the hectorite surfaces separately, in contrast to previous results that show the H_2O molecules located in the mid-plane of the interlayer.[75,76] Nevertheless, the values are in the same range ($0.15 – 0.70 \times 10^{-9} m^2/s$ – monolayer : $1.2 – 1.5 \times 10^{-9} m^2/s$ - bilayer) as reported for the smectite mineral, montmorillonite, using molecular simulation and neutron scattering techniques.[107,113,115] The reported diffusion coefficient of H_2O molecules in bilayer hydrate is slightly higher than previous simulations studies using montmorillonite.[107,113] This difference is probably due to the combination of different substrate structure and associated charge, interaction potentials and substrate flexibility. In addition, the interlayers in previous studies contained only Na^+ ions[113] or 99% Na^+ ions and 1% Cs^+,[107] in contrast to our homoionic Cs^+ hectorite. Despite having interlayer spacings similar to Na- and Ca-hectorites,[73,116] the Cs-hectorite here has larger H_2O diffusion coefficients at all hydration states (Table 2). This difference is probably due to the smaller hydration energy of Cs^+ compared to Na^+ and Ca^{2+}. In contrast, the H_2O diffusion coefficients on the external surfaces do not depend significantly on the counterion, and are all $\sim 3.0 \times 10^{-9}$ m^2/s.[42,43] This value is in excellent agreement with self-diffusion coefficients calculated for bulk SPC water.[42,43,70] However, it should be noted that the diffusion of the H_2O molecules close to the hectorite surface (~<10-15Å) is more restricted because of the presence of charged hectorite surface, as reported by earlier simulation studies on montmorillonite surfaces.[108,109,113,114,117] Since we are focusing on the effect of the

opposing surface on the dynamics of H_2O molecules, the lateral diffusion coefficients as a function of distance from hectorite surface are not reported here.

Site residence times

The intermittent and continuous residence times for three different pairs (Cs^+ - H_2O, Cs^+ - O_b and H_2O – O_b) in Cs-hectorite interlayers (Table 3) are consistent with the results above showing that Cs^+, with its large ionic radius and low hydration energy, prefers to be adsorbed in inner sphere coordination close to the hectorite surface. Both types of mean residence times for all pairs decrease with increasing interlayer hydration, and as expected the intermittent residence times are longer than the continuous residence times. The Cs^+ - O_b residence times are longer than the Cs^+ - H_2O ones, which are longer than the H_2O – O_b ones. This order clearly shows the effects of the low hydration energy of Cs^+ and the relative weakness of H-bonding to the O_b atoms. This result is in direct contrast to the results for Ca-hectorite, which show that the Ca^{2+} - H_2O residence times are more than a factor of 2 greater than the Ca^{2+} - O_b ones due to the higher hydration energy of Ca^{2+}.[116]

Conclusions

Classical MD simulations of the structure, energetics and dynamics of Cs^+ and H_2O in the interlayers of Cs-hectorite clay and on the Cs-hectorite surface using a new hectorite model with a disordered distribution of isomorphic Li^+/Mg^{2+} substitution in the octahedral sheet suggest that only the mono-layer hydrate is stable at ambient pressures and temperatures, in agreement with experimental results. The calculated basal spacings and the H_2O/Cs^+ ratios are in good agreement

with previous experimental and simulation studies. In the interlayer and on the basal surface, Cs^+ ions occur on two different types of inner sphere adsorption sites: (i) at center of the ditrigonal cavities (~2.1 Å from the surface) and (ii) above the Si tetrahedra (~3 Å from the surface). In the monolayer hydrate, Cs^+ ions are hydrated by the H_2O molecules that are coordinated to the opposite surface confining the interlayer, but not by those that share the same plane. For all hydration states, the near surface adsorbed H_2O molecules are oriented in a manner in which they donate ~1 H-bond to the hectorite surface, with the second H_{H2O} being donated to other H_2O molecules. The H_2O structural arrangements at the external basal surface are very similar except for a shoulder at $z < 2.0$ Å, which represents H_2O molecules adsorbed at the center of ditrigonal cavities with both H_{H2O} coordinating the surface. The angular distributions of the H_2O molecules contributing to the peak at 2.6 Å in the atomic density profiles have their dipoles oriented towards the surface, in contrast to the results of previous simulations.[75,76] We attribute the differences between our study and previous simulations to a combination of different structural charges on the clay, different interatomic potentials and our use of the CLAYFF force field, which allows the atoms in the clay substrate to move. Most importantly, this flexibility allows the H-atoms of the structural –OH groups of the clay to reorient to be more parallel to the clay layers rather remaining perpendicular to the surface as in previous simulations with a rigid substrate model. This change reduces the $-OH\cdots O_{H2O}$ attraction and allows Cs^+ ions to be coordinated in the centers of hexagonal rings. The calculated interlayer H_2O diffusion coefficients are generally similar to previous studies and are smaller than on external surfaces. The residence time correlation functions for the pairs Cs^+ - H_2O, Cs^+ - O_b and H_2O – O_b show that the Cs^+ - O_b residence times are longer than the Cs^+ - H_2O ones, which are longer than the H_2O – O_b ones. This order reflects the low hydration energy of Cs^+ and the relative weakness of H-bonding to the O_b atoms. It is in direct

contrast to the results for Ca-hectorite, which show that the Ca^{2+} - H_2O residence times are more than a factor of 2 greater than the Ca^{2+} - O_b ones due to the higher hydration energy of Ca^{2+}.

ACKNOWLEDGMENTS

All the calculations in this work were performed using computational resources at the National Energy Research Scientific Computing Center, which is supported by the Office of Science of the U.S. Department of Energy under ECARP No. m1649. This research is supported by U.S. Department of Energy Office of Basic Energy Sciences to Michigan State University under the grant DE-FG02-08ER15929 (R. J. Kirkpatrick, P.I.) and supported by U.S. DOE grant DE-FG0210ER16128 at Alfred University (G.M. Bowers, P.I.). AGK acknowledges the support of the industrial chair "Storage and Disposal of Radioactive Waste" at the Ecole des Mines de Nantes, funded by ANDRA, Areva, and EDF.

ASSOCIATED CONTENT

Supporting Information. Details of H-Bonding Structure and planar atomic density distributions (PADDs) of near surface adsorbed H_{H2O} for mono and bilayer hydrate, 1^{st} O_{H2O} peak for the external basal surface.

Notes

The authors declare no competing financial interest.

REFERENCES

1. Fenter, P.; Sturchio, N. C. Mineral-Water Interfacial Structures Revealed by Synchrotron X-ray Scattering. *Progr. Surf. Sci.* **2004**, *77*, 171-258.
2. Higgins, J. M.; Polcik, M.; Fukuma, T.; Sader, E. J.; Nakayama, Y; Jarvis, P. S. Structured Water Layers Adjacent to Biological Membranes. *Biophys. Journal* **2006**, *91*, 2532-2542.
3. Israelachvili, J.; Pashley, R. The Hydrophobic Interaction is Long-Range, Decaying Exponentially with Distance. *Nature* **1982**, *300*, 341-342.
4. Rutter, H. E.; Maddock, H. R.; Hall, H. S.; White, H. S. Comparative Microstructures of Natural and Experimentally Produced Clay-Bearing Fault Gouges. *Pure Appl. Geophys*. **1986**, *124*, 3-30.
5. Schlegel, L. M.; Nagy, L. K.; Fenter, P.; Cheng, L.; Sturchio, C. N.; Jacobsen, D. S. Cation Sorption on the Muscovite (001) Surface in Chloride Solutions Using High-Resolution X-ray Reflectivity. *Geochim. Cosmochim. Acta* **2006**, *70*, 3549-3565.
6. Davis, A. J.; Kent, B. D. Surface Complexation Modeling in Aqueous Geochemistry. *Rev. Mineral.* **1990**, *23*, 177-260.
7. Ochs, M.; Boonekamp, M.; Wanner, H.; Satp, H.; Yui, M. A Quantitative Model for Ion Diffusion in Compacted Bentonite. *Radiochim. Acta* **1998**, *82*, 437-444.
8. Park, C.; Fenter, P.; Nagy, L. K.; Sturchio, C. N. Hydration and Distribution of Ions at the Mica-Water Interface. *Phys. Rev. Lett*. **2006**, *97*, 16101-
9. Brown, E. G.; Henrich, E. V.; Casey, H. W.; Clark, L. D.; Eggleston, C., Felmy, A.; Goodman, W.; Gratzel, M.; Maciel, G.; McCarthy, I. M.; Nealson, H. K.; Sverjensky, A. D., Toney, F. M.; Zachara, M. J. Metal Oxide Surfaces and Their Interactions with Aqueous Solutions and Microbial Organisms. *Chem. Rev.* **1998**, *99*, 77-174.
10. Weiss, C. A.; Kirkpatrick, R. J.; Altaner, S. P. Variations in Interlayer Cation Sites of Clay Minerals as Studied by ^{133}Cs MAS Nuclear Magnetic Resonance Spectroscopy. *Amer. Mineral.* **1990**, *75*, 970-982.
11. Marklund, L.; Simic, E.; Worman,A.; Dverstorp, B. The Impact of Different Geological Parameters on Transport of Radionuclides. In Proceedings of 2006 International High-Level Radioactive Waste Management Conference; American Nuclear Society, Las Vegas, NV, 36-373.
12. Bodvarsson, G. S.; Boyle, W.; Patterson, R.; Williams, D. Overview of Scientific Investigations at Yucca Mountain – The Potential Repository for High-Level Nuclear Waste. *J. Contam. Hydrol.* **1999**, *38*, 3-24.
13. Long, J. C. S.; Ewing, R. C. Yucaa Mountain: Earth-Sciences Issues at a Geological Repository for High-Level Nuclear Waste. *Ann. Rev. Earth Planet Sci.* **2004**, 32, 363-401.
14. Vieillard, P.; Ramirez, S.; Bouchet, A, A.; Cassagnabere, A.; Meunier, A.; Jacquot, E. Alteration of the Callovo-Oxfordian Clay from Meuse-Haute Marne Underground Laboratory (France) by Alkaline Solution: II Modeling of Mineral Reactions. *Appl. Geochem.* **2004**, *19*, 1699-1709.

15. Altmann, S.; Tournassat, C.; Goutelard, F.; Parneix, J. C.; Gimmi, T.; Maes, N. Diffusion-Driven Transport in Clayrock Formations. *Appl. Geochem.* **2012**, *27*,463-478.

16. Rubin, E. S. CO_2 Capture and Transport. *Elements* **2008,** *4*, 311-317.

17. Lackner, K. S. A Guide to CO_2 Sequestration. *Science* **2003,** *300*, 1677-1678.

18. Benson, S. M.; Cole, D. R. CO_2 Sequestration in Deep Sedimentary Formations. *Elements* **2008,** 4, 325-331.

19. Koretsky, C. The Significance of Surface Complexation Reactions in Hydrological Systems: A Gecohemist's Perspective. *J. Hydrol.* **2000**, *230*, 127-171.

20. Brown, G. E.; Calas, G. Environmental Mineralogy – Understanding Element Behavior in Ecosystems. *C. R. Geosci.* **2011**, *343*, 90-112.

21. Meakin, P.; Tartakovsky, A. M. Modeling and Simulation of Pore-Scale Multiphase Fluid Flow and Reactive Transport in Fractured and Porous Media. *Rev. Geophys.* **2009**, 47, RG3002.

22. Henderson, M. A. The Interaction of Water with Solid Surfaces: Fundamental Aspects Revisited. *Surf. Sci. Rep*. **2002**, *46*, 1-308.

23. Wang, J.; Kalinichev, A. G.; Kirkpatrick, R. J. Effects of Substrate Structure and Composition on the Structure, Dynamics and Energetics of Water at Mineral Surfaces: A Molecular Dynamics Modeling Study. *Geochim. Cosmochim. Acta* **2006,** *70*, (3), 562-582.

24. Lee, S. S.; Fenter, P.; Park, C.; Sturchio, N. C.; Nagy, K. L. Hydrated Cation Speciation at the Muscovite (001) Water Interface. *Langmuir* **2010,** *26*, 16647-16651.

25. Malani, A.; Ayappa, K. G. Adsorption Isotherms of Water on Mica: Redistribution and Film Growth. *J. Phys. Chem B* **2009,** *113*, 1058-1067.

26. Sposito, G.; Park, S. H.; Sutton, R. Monte Carlo Simulation of the Total Radial Distribution Function of Interlayer Water in Sodium and Potassium Montmorillonites. *Clays Clay Miner.* **1999**, *47*, 192-200.

27. Montavon, G.; Guo, Z.; Tournassat, C.; Grambow, B.; Le Botlan, D. Porosities Accessible to HTO and Iodide on Water-Saturated Compacted Clay Minerals and Relation with the forms of Water: A Low Field Proton NMR Study. *Geochim. Cosmochim. Acta* **2009,** *73*, 7290-7302.

28. Appelo, C. A.; Wersin, P. Multicomponent Diffusion Modeling in Clay Systems with Application to the Diffusion of Tritium, Iodide and Sodium in Opalinus Clay. *Environ. Sci. Technol.* **2007**, *41*, 5002-5007.

29. Lee, S. S.; Park, C.; Fenter, P.; Sturchio, N. C.; Nagy, K. L. Competitive Adsorption of Strontium and Fulvic Acid at the Muscovite Solution Interface Observed with Resonant Anomalous X-ray Reflectivity. *Geochim. Cosmochim. Acta* **2010,** *74*, 1762-1776.

30. Miranda, P. B.; Xu, L.; Shen, Y. R.; Salmeron, M. Icelike Water Monolayer Adsorbed on Mica at Room Temperature. *Phys. Rev. Lett.* **1998,** *81*, 5876-5879.

31. Kim, Y.; Kirkpatrick, R. ^{23}Na and ^{133}Cs NMR study of Cation Adsorption on Mineral Surfaces: Local Environments, Dynamics and Effects of Mixed Cations. *Geochim. Cosmochim. Acta* **1997,** *61*, 5199-5208.

32. Lee, S. S.; Park, C.; Fenter, P.; Sturchio, N. C.; Nagy, K. L. Monovalent Ion Adsorption at the Muscovite (001) - Solution Interface: Relationships among Ion Coverage and Speciation, Interfacial Water Structure and Substrate Relaxation. *Langmuir* **2012,** *28*, 8637-8650.

33. Moyes, L. N.; Parkman, R. H.; Charnock, J. M.; Vaughan, D. J.; Livens, F. R.; Hughes, C. R.; Braithwaite, A. Uranium Uptake from Aqueous Solution by Interaction with Goethite, Lepidocrocite, Muscovite and Mackinawite: An X-ray Adsorption Spectroscopy Study. *Environ. Sci. Technol.* **2000**, *34*, 1062-1068.

34. Mooney, R. W.; Keenan, A. G.; Wood, L. A. Adsorption of Water Vapor by Montmorillonite. II. Effect of Exchangeable Ions and Lattice Swelling as Measure by X-ray Diffraction. *J. Am. Chem. Soc.* **1952**, *74*, 1371-1374.

35. Hensen, E. J. M.; Smit, B. Why Clays Swell. *J. Phys. Chem. B* **2002**, *106*, 12664-12667.

36. Calvet, R. Hydration of Montmorillonite and Diffusion of Exchangeable Cations. 1. Hydration of Montmorillonite Saturated by Monovalent Cations. *Ann. Agron.* **1973**, *24*, 77-133.

37. Calvet, R. Hydration of Montmorillonite and Diffusion of Exchangeable Cations. 2. Diffusion of Exchangeable Cations in Montmorillonite. *Ann Agron.* **1973**, *24*, 135-217.

38. Bowers, G. M.; Hoyt, D. W.; Burton, S. D.; Ferguson, B. O.; Varga, R.; Kirkpatrick, R. J. In Situ ^{13}C and ^{23}Na Magic Angle Spinning NMR Investigation of Supercritical CO_2 Incorporation in Smectite-Natural Organic Matter Composites. *J. Phys. Chem C* **2014,** *118*, 3564-3573.

39. Wang, J.; Kalinichev, A. G.; Kirkpatrick, R. J.; Cygan, R. T. Structure, Energetics and Dynamics of Water Adsorbed on the Muscovite (001) Surface: A Molecular Dynamics Simulation. *J. Phys. Chem B* **2005,** *109*, 15893-15905.

40. Malani, A.; Ayappa, K. G.; Murad, S. Adsorption Isotherms of Water on Mica: Redistribution and Film Growth. *J. Phys. Chem B* **2009,** *113*, 1058-1067.

41. Feibelman. P. J. K^+-Hydration in a Low-Energy Two-Dimensional Wetting Layer on the Basal Surface of Muscovite. *J. Chem. Phys.* **2013,** *139*, 074705.

42. Loganathan, N.; Kalinichev, A. G. On the hydrogen bonding structure at the aqueous interface of ammonium-substituted mica: A molecular dynamics simulation. *Zeitschrift fur Naturforschung* **2013,** *68a*, 91-100.

43. Rotenberg, B.; Marry, V.; Malikova, N.; Turq, P. Molecular Simulation of Aqueous Solutions at Clay Surfaces. *J. Phys. Condens. Matter* **2010**, *22*, 284114.

44. Boek, E. S.; Sprik, M. Ab Initio Molecular Dynamics Study of the Hydration of a Sodium Smectite Clay. *J. Phys. Chem B* **2003,** *107*, 3251-3256.

45. Bowers, G. M.; Bish, D. L.; Kirkpatrick, R. J. Cation Exchange at the Mineral-Water Interface: H_3O^+/K^+ Competition at the Surface of Nano-Muscovite. *Langmuir* **2008**, *24*, 10240-10244.

46. Gomez, S. A. S.; Jordan, D. S.; Troiano, J. M.; Geiger, F. M. Uranyl Adsorption at the Muscovite (Mica)/Water Interface Studied by Second Harmonic Generation. *Environ. Sci. Technol.* **2012**, *46*, 11154-11161.

47. Greathouse, J. A.; Cygan, R. T. Water Structure and Aqueous Uranyl (VI) Adsorption Equilibria onto External Surfaces of Beidellite, Montmorillonite and Pyrophyllite: Results from Molecular Simulations. *Environ. Sci. Technol.* **2006**, *40*, 3865-3871.

48. Teich-McGoldrick, S. L.; Greathouse, J. A. Molecular Dynamics Simulations of Uranyl Adsorption and Structure on the Basal Surface of Muscovite. *Molecular Simulations*, **2014**, *40*, 610-617.

49. Kerisit, S.; Liu, C. Molecular Dynamics Simulations of Uranyl and Uranyl Carbonate Adsorption at Aluminosilicate Surfaces. *Environ. Sci. Technol.* **2014**, *48*, 3899-3907.

50. Ngouana-Wakou, B. F.; Kalinichev, A. G. Structural Arrangements of Isomorphic Substitutions in Smectites: Molecular Simulation of the Swelling Properties, Interlayer Structure and Dynamics of Hydrated Cs-Montmorillonite Revisited with New Clay Models. *J. Phys. Chem. C* **2014**, *118*, 12758-12773.

51. Reinholdt, M. X.; Kirkpatrick, R. J.; Pinnavaia, T. J. Montmorillonite-Poly(ethylene oxide) Nanocomposites: Interlayer Alkali Metal Behavior. *J. Phys. Chem B* **2005,** *109*, 16296-16303.

52. Sato, T.; Watanabe, T.; Otuka, R. Effects of Layer Charge, Charge Location, and Energy Change on Expansion Properties of Dioctahedral Smectites. *Clays Clay Miner.* **1992**, *29*, 873-882.

53. Gournis, D.; Lappas, A.; Karakassides, M.; Tobbens, D.; Moukarika, A. A Neutron Diffraction Study of Alkali Cation Migration in Montmorillonites. *Phys. Chem. Miner.* **2008**, *35*, 49-58.

54. Liu, X.; Lu, X.; Wang, R.; Zhou, H. Effects of Layer-Charge Distribution on the Thermodynamic and Microscopic Properties of Cs-Smectite. *Geochim. Cosmochim. Acta* **2008**, *72*, 1897-1847.

55. Whitley, H. D.; Smith, D. E. Free Energy, Energy and Entropy of Swelling in Cs-,Na- and Sr-Montmorillonite Clays. *J. Phys. Chem B* **2004,** *120*, 5387-5395.

56. Devinearu, K.; Bihannic, I.; Michot, L.; Villieras, F.; Masrouri, F.; Cuisinier, O.; Fragneto, G.; Michau, N. In Situ Neutron Diffraction Analysis of the Influence of Geometric Confinement on Crystalline Swelling of Montmorillonite. *Appl. Clay. Sci.* **2006**, *31*, 76-84.

57. Boulet, P.; Bowden, A. A.; Coveney, P. V.; Whiting, A. Combined Experimental and Theoretical Investigations of Clay Polymer Nano-Composites: Intercalation of Single Bifunctional Organic Compounds in Na^+Montmorillonite and Na^+Hectorite Clays for the Design of New Materials. *J. Mater. Chem.* **2003**, *13*, 2540-2550.

58. Yazaydin, A. O.; Bowers, G. M.; Kirkpatrick, R. J. Molecular Dynamics Modeling of Carbon dioxide, Water and Natural Organic Matter in Na-Hectorite. *Phys. Chem. Chem. Phys*. **2015**, *17*, 23356-23367.

59. Bowers, G. M.; Singer, J. W.; Bish, D. L.; Kirkpatrick, R. J. Alkali Metal and H_2O Dynamics at the Clay/Water Interface. *J. Phys. Chem. C* **2011**, *115*, 23395-23407.

60. Annabi-Bergaya, F.; Estrade-Szwarckopf, H.; Damme, V, H. Dehydration of Cu-Hectorite: Water Isotherm, XRD and EPR Studies. *J. Phys. Chem.* **1996**, *100*, 4120-4126.

61. Karmous, M. S.; Oueslati, W.; Ben Rhaiem, H.; Robert, J. L., Amara, A. B. H. Simulation of the XRD Patterns, Structural Properties of a Synthetic Na-Hectorite Exchange Cu(2+) and Ca (2+). *Z. Kristallogr.* **2007**, *26*, 503-508.

62. Weiss, C. A.; Kirkpatrick, R. J.; Altaner, S. P. The Structural Environments of Cations Adsobed onto Clays – Cs 133 Variable Temperature MAS NMR Spectroscopic Study of Hectorite. *Geochim. Cosmochim. Acta* **1990**, *54*, 1655-1669.

63. Kalo, H.; Milius, W.; Breu, J. Single Crystal Structure Refinement of One- and Two-Layer Hydrates of Sodium Fluorohectorite. *RSC Adv.* **2012**, *2*, 8452-8459.

64. Michot, L. J.; Ferrage, E.; Jimenez-Ruiz.; Boehm, M.; Delville, A. Anisotropic Features of Water and Ion Dynamics in Synthetic Na- and Ca-Smectites with Tetrahedral Layer Charge. A Combined Quasi-Elastic Neutron-Scattering and Molecular Dynamics Simulations Study. *J. Phys. Chem. C* **2012**, *116*, 16619-16633.

65. Marry, V.; Dubois, E.; Malikova, N.; Durand-Vidal, S.; Longeville, S.; Breu, J. Water Dynamics in Hectorite Clays: Influence of Temperature Studied by Coupling Neutron Spin Echo and Molecular Dynamics. *Environ. Sci. Technol.* **2011**, *45*, 2850-2855.

66. Sobolev, O.; Le Forestier, L.; Gonzalez, M. A.; Russina, M.; Kemner, E.; Cuello, G. J.; Charlet, L. Hydration of $Na^{+,}$ Ni^{2+} and Sm^{3+} in the Interlayer of Hectorite: A Quasi Neutron Scattering Study. *J. Phys. Chem. C* **2009**, *113*, 13801-13812.

67. Marry, V.; Malikova, N.; Cadene, A.; Dubois, E.; Durand-Vidal, S.; Turq, P.; Breu, J.; Longeville, S.; Zanotti, J. M. Water Diffusion in a Synthetic Hectorite by Neutron Scattering – Beyond the Isotropic Translational Model. *J. Phys.: Condens. Matter* **2008**, *20*, 104205.

68. Bowers, G. M.; Bish, D. L; Kirkpatrick, R. J. H_2O and Cation Structure and Dynamics in Expandable Clays: ^{2}H and ^{39}K NMR Investigations of Hectorite. *J. Phys. Chem. C* **2008**, *112*, 6430-6438.

69. Porion, P.; Faugere, A. M.; Delville, A. Multiscale Water Dynamics within Dense Clay Sediments Probed by 2H Multiquantum NMR Relaxometry and Two-Time Stimulated Echo NMR Spectroscopy. *J. Phys. Chem. C* **2013**, *117*, 26119-26134.

70. Porion, P.; Warmont, F.; Faugere, A. M.; Rollet, A-L.; Dubois, E.; Marry, V.; Michot, L. J.; Delville, A. 133Cs Nuclear Magnetic Resonance Relaxometry as a Probe of the Mobility of Cesium Cations Confined within Dense Clay Sediments. *J. Phys. Chem. C* **2015**, *119*, 15360-15372.

71. Bowers, G. M.; Singer, J. W.; Bish, D. L.; Kirkpatrick, R. J. Structure and Dynamical Relationships of Ca^{2+} and H_2O in Smectite/$^{2}H_2O$ Sytems. *Amer. Mineral*. 2014, *99*, 318-331.

72. Hartzell, C. J.; Cygan, R. T.; Nagy, K. L. Molecular Modeling of Tributyl Phosphate Complex of Europium Nitrate in the Clay Hectorite. *J. Phys. Chem. A* **1998**, *102*, 6722-6729.

73. Morrow, C. P.; Yazaydin, A. O.; Krishnan, M.; Bowers, G. M.; Kalinichev, A. G.; Kirkpatrick. R. J. Structure, Energetics and Dynamics of Smectite Clay Interlayer Hydration: Molecular Dynamics and Metadynamics Investigation of Na-Hectorite. *J. Phys. Chem. C* **2013**, *117*, 5172-5187.

74. Greathouse, J. A.; Hart, D. B.; Bowers, G. M.; Kirkpatrick, R. J.; Cygan, R. T. Molecular Simulation of Structure and Diffusion at Smectite-Water Interfaces: Using Expanded Clay Interlayers as Model Nanopores. *J. Phys. Chem. C* **2015**, *119*, 17126-17136.

75. Sutton, R.; Sposito, G. Animated Molecular Dynamics Simulations of Hydrated Caesium-Smectite Interlayers. *Geochem. Trans.* **2002**, *3*, 73-80.

76. Sutton, R.; Sposito, G. Molecular Simulation of Interlayer Structure and Dynamics in 12.4Å Cs-Smectite Hydrates. *J. Coll. Interf. Sci*. **2001**, *237*, 174-184.

77. Flury, M.; Gimmi, T. F. Solute Diffusion. In Methods of Soil Analysis Part 4: Physical Methods; Dane, J. H., Topp, G. C., Eds.; Soil Science Society of America: Madison, WI, **2002**; pp 1323-1351.

78. Okumura, M.; Nakamura, H.; Machida, M. Mechanism of Strong Affinity of Clay Minerals to Radioactive Cesium: First-Principles Calculation Study for Adsorption of Cesium at Frayed Edge Sites in Muscovite. *J. Phys. Soc. Jpn.* **2013**, *82*, 033802.

79. Yasanuri, T. J.; Stohl, A.; Hayano, R. S.; Burkhart, J. F.; Eckhardt, S.; Yasanuri, T. Cesium-137 Deposition and Contamination of Japanese Soils Due to the Fukushima Nuclear Accident. *Proc. Natl. Acad. Sci.* U.S.A. **2011**, *108*, 19530-19534.

80. Bostick, B. C.; Vairavamurthy, M. A.; Karthikeyan, K. G.; Chorover, J. Cesium Adsorption of Clay Minerals: An EXAFS Spectroscopic Investigation. *Environ. Sci. Technol.* **2002**, *36*, 2670-2676.

81. Fan, Q.; Yamaguchi, N.; Tanaka, M.; Tsukada, H.; Takahashi, Y. Relationship Between the Adsorption Species of Cesium and Radiocesium Interception Potential in Soils and Minerals : An EXAFS Study. *J. Environ. Radio.* **2014,** *138*, 92-100.

82. Nakano, M.; Kawamura, K.; Ichikawa, Y. Local Structural Information of Cs in Smectite Hydrates by Means of an EXAFS Study and Molecular Dynamics Simulations. *Appl. Clay. Sci.* **2003**, *23*, 15-23.

83. Ferguson, B. O.; Arey, B.; Varga, T.; Burton, S.; Bowden, M.; Argersinger, H. E.; Kirkpatrick, R. J.; Bowers, G. M. X-ray Diffraction and Helium ion and Electron Microscopy of Smectite-Natural Organic Matter Composites. *Clays Clay Minerals* **(Submitted)**

84. Reddy, U. V. ; Bowers, G. M.; Loganathan, N.; Bowden, M. ; Yazaydin, A. O.; Kirkpatrick, R. J. Water Structure and Dynamics in Smectites: ^{2}H NMR Spectroscopy of Mg, Ca, Sr, Cs and Pb-Hectorite. *J. Phys. Chem. C* **2016**, DOI: 10.1021/acs.jpcc.6b03431.

85. Breu, J.; Seidl, W.; Stoll, A. Disorder in Smectites in Dependence of the Interlayer Cation. Z. *Anorg. Allg. Chem*. **2003**, *629*, 503-515.

86. Tenorio, R. P.; Alme, L. R.; Engelsberg, M.; Fossum, J. O.; Hallwass, F. Geometry and Dynamics of Intercalated Water in Na-Fluorohectorite Clay Hydrates. *J. Phys. Chem C* **2008**, *112*, 575-580.

87. Plimpton, S. Fast Parallel Algorithms for Short-Range Molecular Dynamics. *Journal of Computational Physics* **1995,** *117*, (1), 1-19.

88. Shinoda, W.; Shiga, M.; Mikami, M. Rapid Estimation of Elastic Constants by Molecular Dynamics Simulations under Constant Stress. *Phys. Rev. B.* **2004,** *69*, 134103.

89. Tuckerman, M. E.; Alejandre, J.; Rendon, R.; Jochim, A. A.; Martyna, G. J. Liouville-Operator Derived. Measure-Preserving Integrator for Molecular Dynamics Simulations in the Isothermal-Isobaric Ensemble. *J. Phys. A: Math. Gen.* **2006,** *39*, 5629-5651.

90. Cygan, R. T.; Liang, J.-J.; Kalinichev, A. G. Molecular Models of Hydroxide, Oxyhydroxide and Clay Phases and the Development of a General Force Field. *J. Phys. Chem. B* **2004,** *108*, 1255-1266.

91. Narasimhan, L.; Boulet, P.; Kuchta, B.; Schaef, O.; Denoyel, R.; Brunet, P. Molecular Simulations of Water and Paracresol in MFI Zeolite – A Monte Carlo Study. *Langmuir* **2009**, *25*, 11598-11607.

92. Narasimhan, L.; Kuchta, B.; Schaef, O.; Brunet, P.; Boulet, P. Mechanism of Adsorption of p-cresol Uremic Toxin into Faujasite Zeolites in Presence of Water and Sodium Ions – A Monte Carlo Study. *Micro. Meso. Mat*. **2013**, *173*, 70-77.

93. Berendsen, H. J. C.; Postma, J. P. M.; van Gunsteren, W. F.; Hermans, J. Interaction Models for Water in Relation to Protein Hydration. In: *Intermolecular Forces*, Pullman, B., Ed.; Riedel: Dordrecht, The Netherlands, **1981**; 331-342.

94. Smith, D. E. Molecular Computer Simulations of the Swelling Properties and Interlayer Structure of Cesium Montmorillonite. *Langmuir* **1998**, *14*, 5959-5967.

95. Bickmore, B. R.; Rosso, K. M.; Brown, I. D.; Kerisit, S. Bond-Valence Constraints on Liquid Water Structure. *J. Phys. Chem. A* **2009**, *113*, 1847-1857.

96. Benjamin, I. Chemical Reactions and Solvations at Liquid Interfaces: A Microscopic Perspective. *Chem. Rev.* **1996**, *96*, 1449-1475.

97. Chowdhuri, S.; Chandra, A. Dynamics of Halide Ion-Water Hydrogen Bonds in Aqueous Solutions: Dependence on Ion Size and Temperature. *J. Phys. Chem. B* **2006**, *110*, 9674-9680.

98. Luzar, A.; Chandler, D. Hydrogen-bond Kinetics in Liquid Water. *Nature* **1996**, *379*, 55-57.

99. Impey, R. W.; Madden, P. A.; McDonald, I. R. Hydration and Mobility of Ions in Solution. *J. Phys. Chem.* **1983**, *87*, 5071-5083.

100. Luzar, A. Resolving the Hydrogen Bond Dynamics Conundrum. *J. Chem. Phys*. **2000**, *113*, 10663.

101. Iskrenova-Tchoukova, E.; Kalnichev, A. G.; Kirkpatrick, R. J. Metal Cation Complexation with Natural Organic Matter in Aqueous Solutions: Molecular Dynamics Simulations and Potentials of Mean Force. *Langmuir* **2010**, *26*, 15909-15919.

102. Seidl, W.; Breu, J. Single Crystal Structure Refinement of Tetramethylammonium-Hectorite. *Z. Kristallogr*. **2005**, *220*, 169-176.

103. Kosakowski, G.; Churakov, S. V.; Thoenen, T. Diffusion of Na and Cs in Montmorillonite. *Clays Clay Miner.* **2008**, *56*, 190-206

104. Prost, R.; Koutit, T.; Benchara, A.; Huard, E. State and Location of Water Adsorbed on Clay Minerals: Consequences of the Hydration and Swelling-Shrinkage Phenomena. *Clays Clay Miner*. **1998**, *46*, 117-131.

105. Sposito, G.; Prost, R. Structure of Water Adsorbed on Smectites. *Chem. Rev.* **1982**, *82*, 554-573.

106. Skipper, N. T.; Chang, F-R. C.; Sposito, G. Monte Carlo Simulation of Interlayer Molecular Structure in Swelling Clay Minerals 1. Methodology. *Clays Clay Miner.* **1995**, *43*, 285-293.

107. Marry, V.; Turq. P. Microscopic Simulations of Interlayer Structure and Dynamics in Bihydrated Heteroionic Montmorillonites. *J. Phys. Chem. B.* **2003**, *107*, 1832-1839.

108. Marry, V.; Rotenberg, B.; Turq. P. Structure and Dynamics of Water at a Clay Surface from Molecular Dynamics Simulation. *Phys. Chem. Chem. Phys.* **2008**, *10*, 4802-4813.

109. Churakov, S. Mobility of Na and Cs on Montmorillonite Surface under Partially Saturated Conditions. *Environ. Sci. Technol.* **2013**, *47*, 9816-9823.

110. Loganathan, N.; Kalinichev, A. G.**(Unpublished results)**.

111. Koneshan, S.; Rasaiah, J. C.; Lynden-Bell, R. M.; Lee, S. H. Solvent structure, dynamics and the ion mobility in aqueous solution at 25^{o}C *J. Phys. Chem. B* **1998**, 102, 4193-4204.

112. Ohtaki, H.; Radnai, T. Structure and Dynamics of Hydrated Ions. *Chem. Rev*. **1993,** 93, 1157-1204.

113. Holmboe, M.; Bourg, I. C. Molecular Dynamics Simulationis of Water and Sodium Diffusion in Smectite Interlayer Nanopores as a Function of Pore Size and Temperature. *J. Phys. Chem. C* **2013**, 118, 1001-1013.

114. Bourg, I. C.; Sposito, G. Connecting the Molecular Scale to the Continuum Scale for Diffusion Processes in Smectite-Rich Porous Media. *Environ. Sci. Technol.* **2010**, *44*, 2085-2091.

115. Malikova, N.; Cadene, A., Marry, V.; Dubois, E.; Turq, P.; Zanotti, J. M.; Longeville, S. Diffusion of Water in Clays –Microscopic Simulation and Neutron Scaterring. *Chem. Phys*. **2005**, *317*, 226-235.

116. Loganathan, N.; Yazaydin, A. O.; Bowers, G. M.; Kalinichev, A. G.; Kirkpatrick, R. J. Cation and Water Structure, Dynamics and Energetics in Smectite Clays: A Molecular Dynamics Study of Ca-Hectorite *J. Phys. Chem. C* **(Submitted)**

117. Tournassat, C.; Chapron, Y.; Leroy, P.; Bizi, M.; Boulahya, F. Comparison of Molecular Dynamics Simulations with Triple Layer and Modified Gouy-Chapman Models in a 0.1 M NaCl-Montmorillonite System. *J. Col. Inter. Sci*. **2009**, *339*, 533-541.

FIGURE CAPTIONS

Figure 1. Snapshots of the simulated Cs-hectorite system illustrating the disordered distribution of Li^+/Mg^{2+} substitution in the octahedral sheet. a) View perpendicular to the clay layers. b) External basal surface viewed parallel to the clay layers along the *xy* direction. Purple balls – octahedral Li^+, green balls – octahedral Mg^{2+}, yellow – Si tetrahedra, blue balls – interlayer Cs^+ ions, red sticks – O_{H2O}, white sticks – H_{H2O}. For the sake of clarity the structural OH^- groups are not shown.

Figure 2. Thermodynamic properties of Cs-hectorite as a function of interlayer water content. a) Interlayer spacing. b) Hydration energy. c) Immersion energy. d) Isosteric heats of adsorption. The dashed lines indicate the bulk internal energy of SPC water in b) and the bulk vaporization enthalpy for SPC water in d). The errors bars are at the 90% confidence level.

Figure 3. Atomic density profiles of Cs^+ (gold), O_{H2O} (red), and H_{H2O} for Cs-hectorite as functions of distance from the basal surface for the indicated hydration levels and the external surface. a) Monolayer hydrate. b) Bi-layer hydrate. c) Tri-layer hydrate; d) Basal Surface. The 0 of distance is the mean position of the basal O-atoms of the left surface clay surface.

Figure 4. Orientation distributions of H_2O molecules at the Cs-hectorite interlayers and on the external basal surface. a) Dipole vector of H_2O molecules in the mono-layer hydrate b) HH vector of H_2O molecules in the mono-layer hydrate c) Dipole vector of near surface adsorbed H_2O molecules at the external surface. b) HH vector of near surface adsorbed H_2O molecules at the external surface.

Figure 5. Radial distribution functions (RDFs, solid lines) and corresponding running coordination numbers (RCNs, dashed lines) for a) Cs^+ - H_2O pairs and b) Cs^+ - O_b pairs in the interlayers and on external surfaces of Cs-hectorite. Color code: monolayer hydrate – black, bilayer hydrate – red, trilayer hydrate – green, external basal surface – blue.

Figure 6. Planar atomic density distributions (PADDs) of Cs^+ ions and O_{H2O} in the interlayers and on external surfaces of Cs-hectorite. a) Cs^+ ions and O_{H2O} atoms at distances $z < 3$ Å in the monolayer hydrate. b) schematic representation of the structural arrangement of H_2O (oxygen – red, hydrogen - cyan) molecules and Cs^+ ions (blue) in the monolayer hydrate. c) Cs^+ ions at distances $z < 2.8$ Å and O_{H2O} atoms at $z < 3.1$ Å in the bilayer hydrate. d) Cs^+ ions at $z < 2.8$ Å and O_{H2O} atoms at $z < 2.4$ Å on external basal surfaces. Color code: O_b – gray, Si – yellow, Cs^+ ions at the center of ditrigonal cavities – blue, Cs^+ ions above Si tetrahedron – green, O_{H2O} – red, H_{H2O} – cyan.

FIGURES

a) 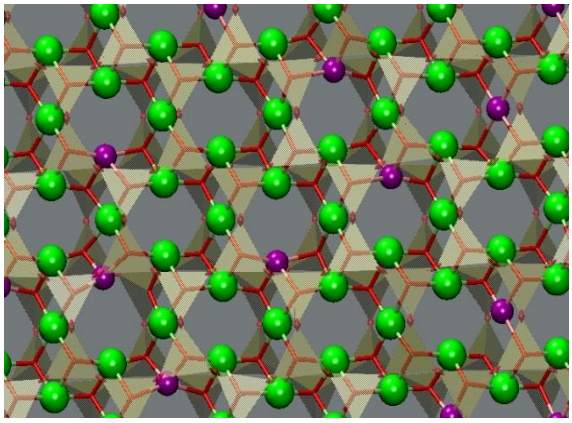 b) 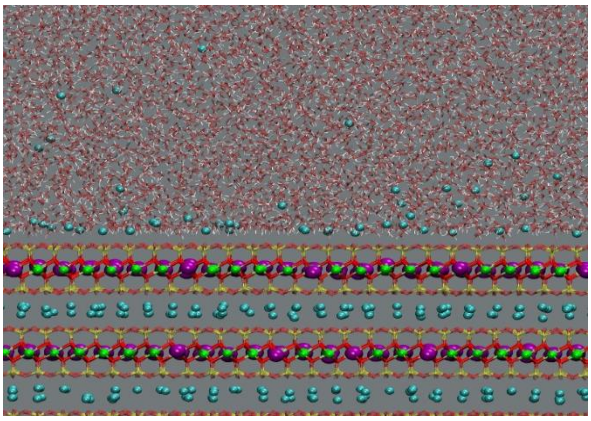

Figure 1. Snapshots of the simulated Cs-hectorite system illustrating the disordered distribution of Li^{+}/Mg^{2+} substitution in the octahedral sheet. a) View perpendicular to the clay layers. b) External basal surface viewed parallel to the clay layers along the *xy* direction. Purple balls – octahedral Li^{+}, green balls – octahedral Mg^{2+}, yellow – Si tetrahedra, blue balls – interlayer Cs^{+} ions, red sticks – O_{H2O}, white sticks – H_{H2O}. For the sake of clarity the structural OH^{-} groups are not shown.

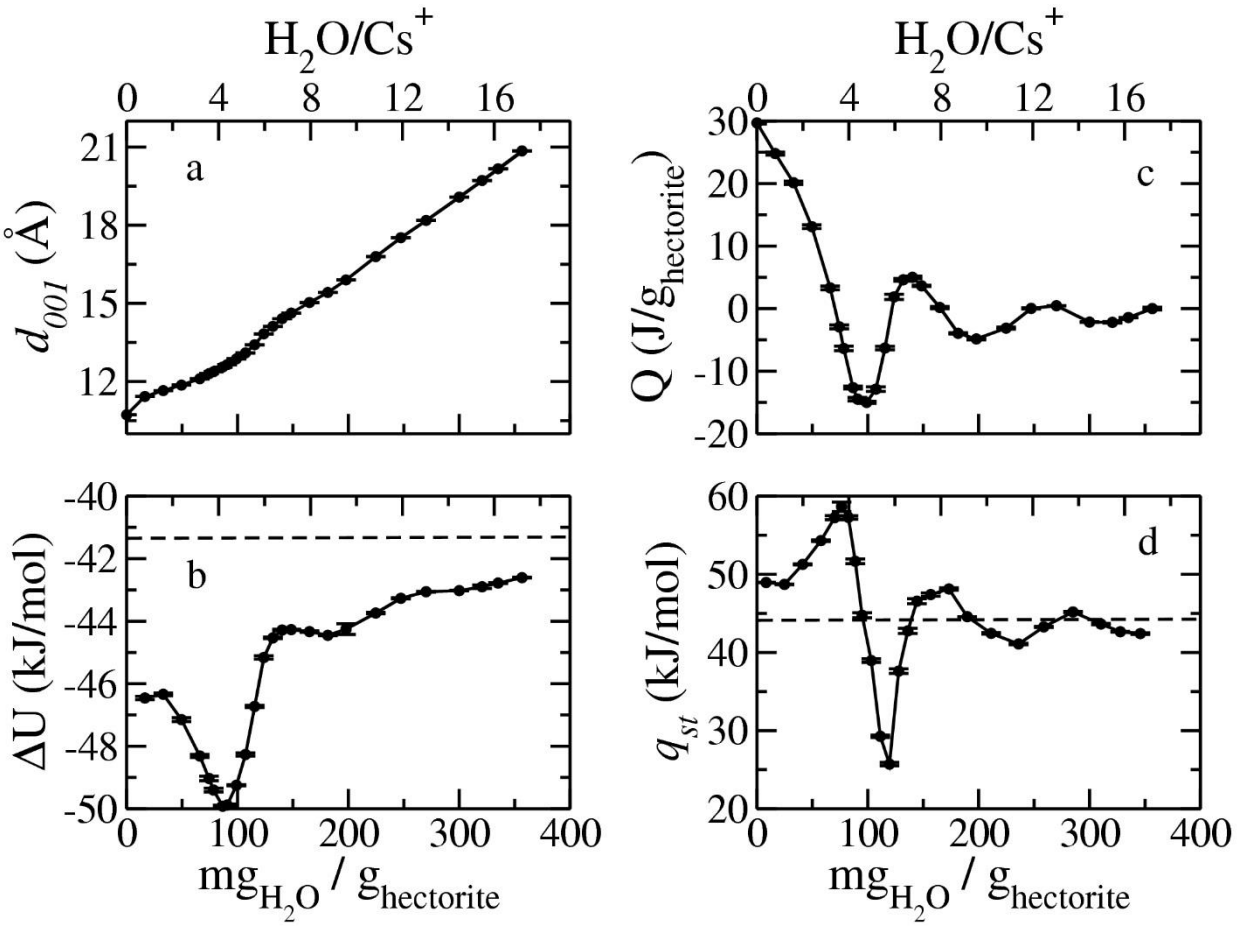

Figure 2. Thermodynamic properties of Cs-hectorite as a function of interlayer water content. a) Interlayer spacing. b) Hydration energy. c) Immersion energy. d) Isosteric heats of adsorption. The dashed lines indicate the bulk internal energy of SPC water in b) and the bulk vaporization enthalpy for SPC water in d). The errors bars are at the 90% confidence level.

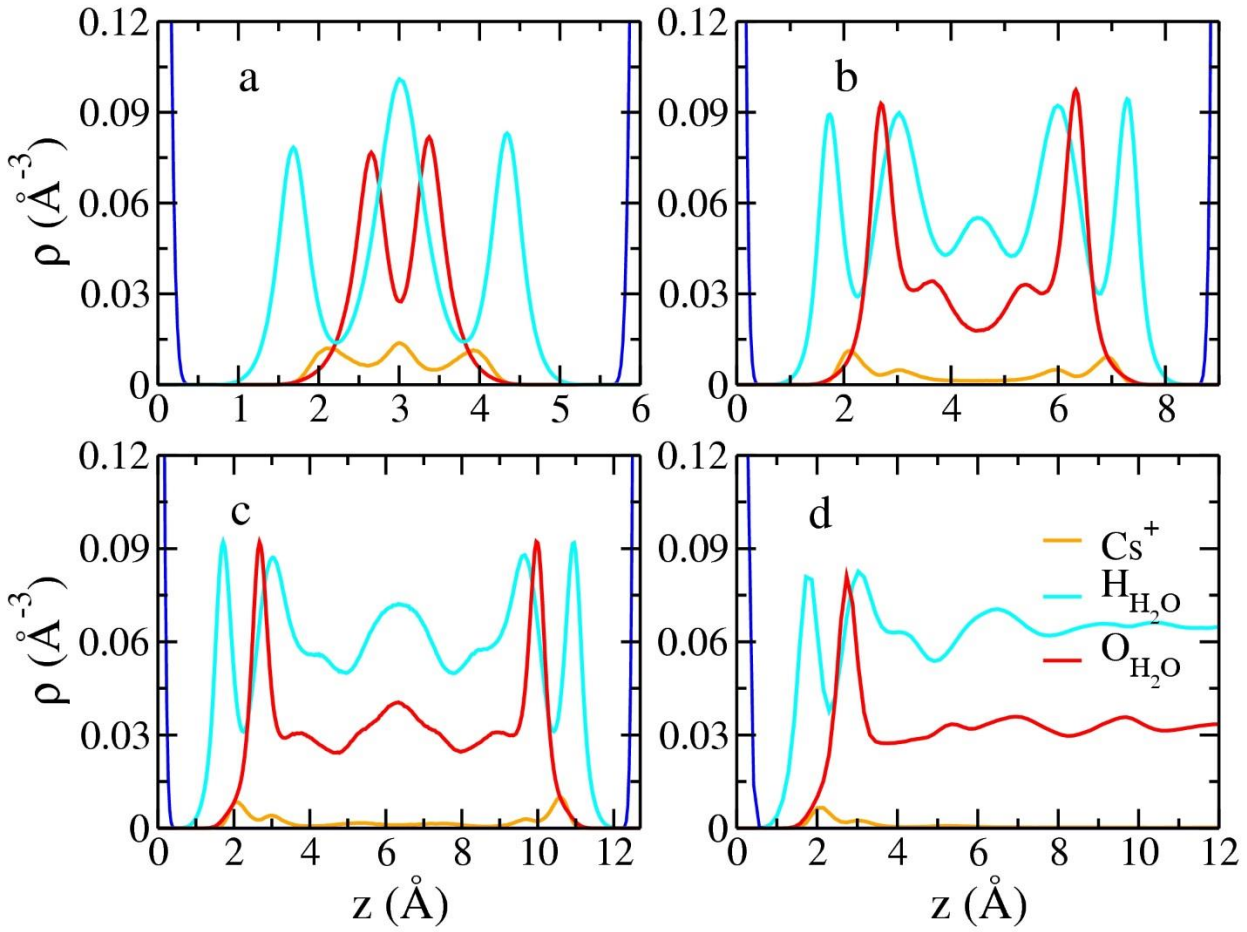

Figure 3. Atomic density profiles of Cs^+ (gold), O_{H2O} (red), and H_{H2O} for Cs-hectorite as functions of distance from the basal surface for the indicated hydration levels and the external surface. a) Monolayer hydrate. b) Bi-layer hydrate. c) Tri-layer hydrate; d) Basal Surface. The 0 of distance is the mean position of the basal O-atoms of the left surface clay surface.

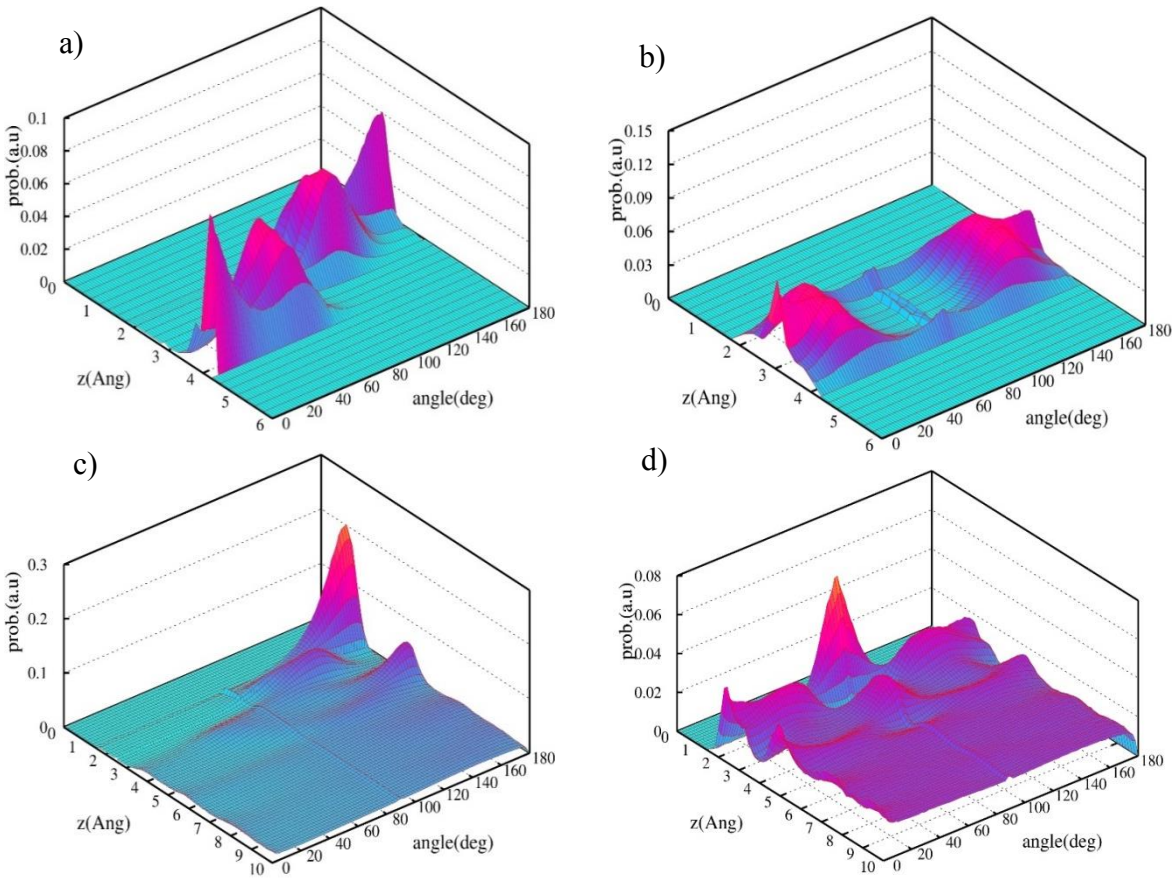

Figure 4. Orientation distributions of H_2O molecules at the Cs-hectorite interlayers and on the external basal surface. a) Dipole vector of H_2O molecules in the mono-layer hydrate b) HH vector of H_2O molecules in the mono-layer hydrate c) Dipole vector of near surface adsorbed H_2O molecules at the external surface. b) HH vector of near surface adsorbed H_2O molecules at the external surface.

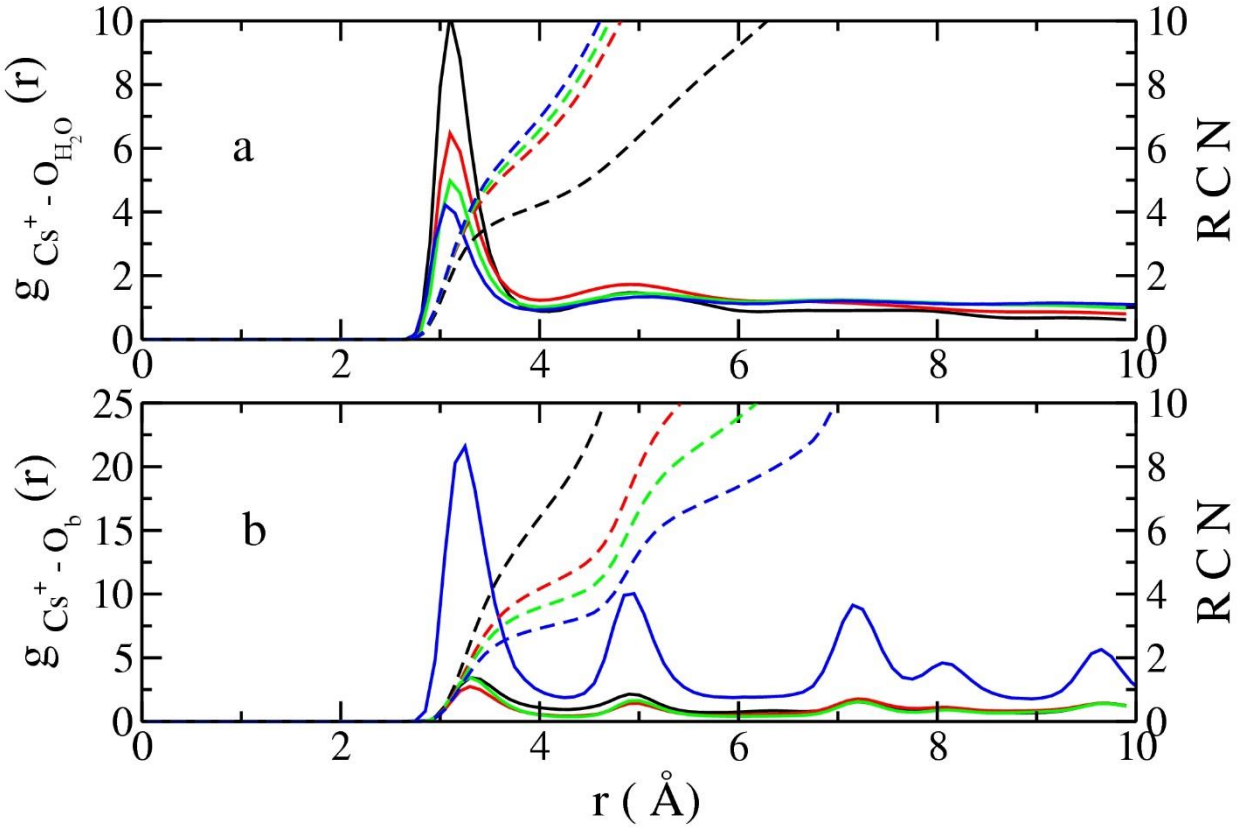

Figure 5. Radial distribution functions (RDFs, solid lines) and corresponding running coordination numbers (RCNs, dashed lines) for a) Cs^+ - H_2O pairs and b) Cs^+ - O_b pairs in the interlayers and on external surfaces of Cs-hectorite. Color code: monolayer hydrate – black, bilayer hydrate – red, trilayer hydrate – green, external basal surface – blue.

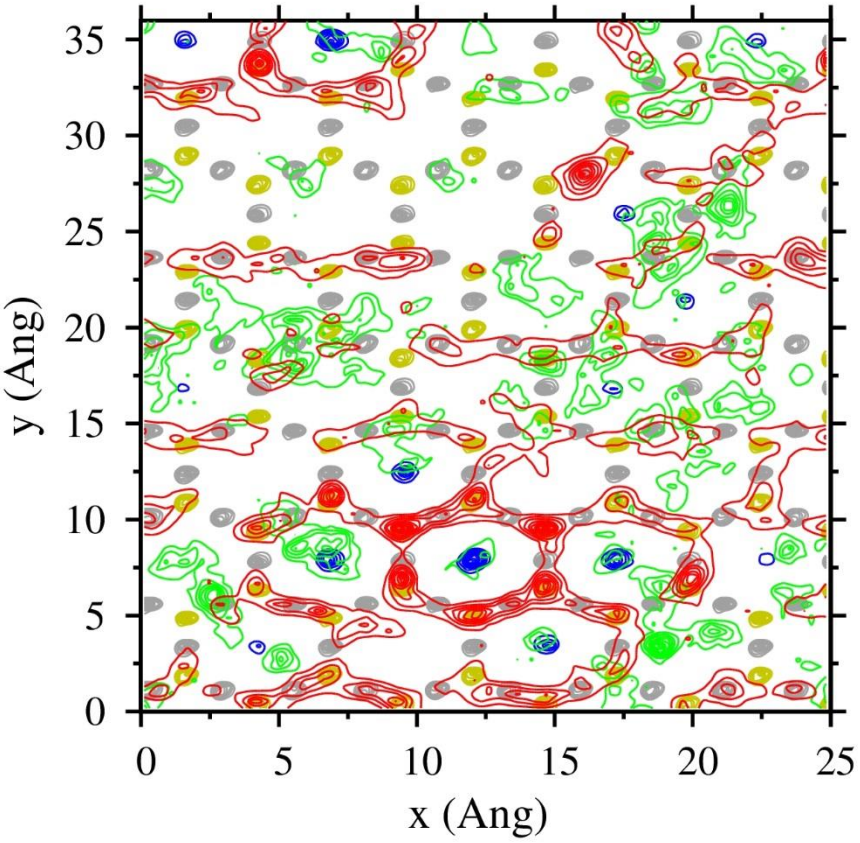

a)

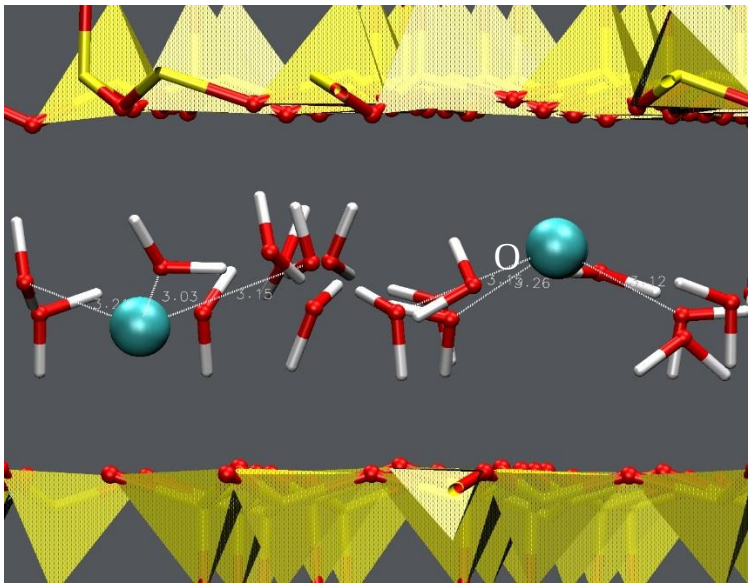

b)

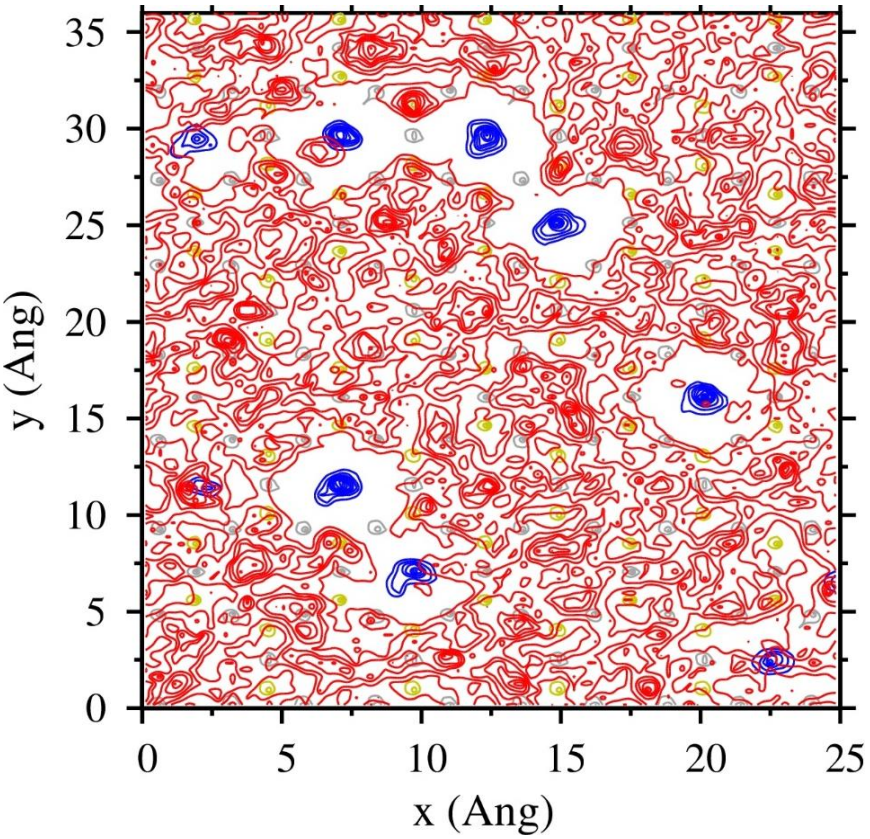

c)

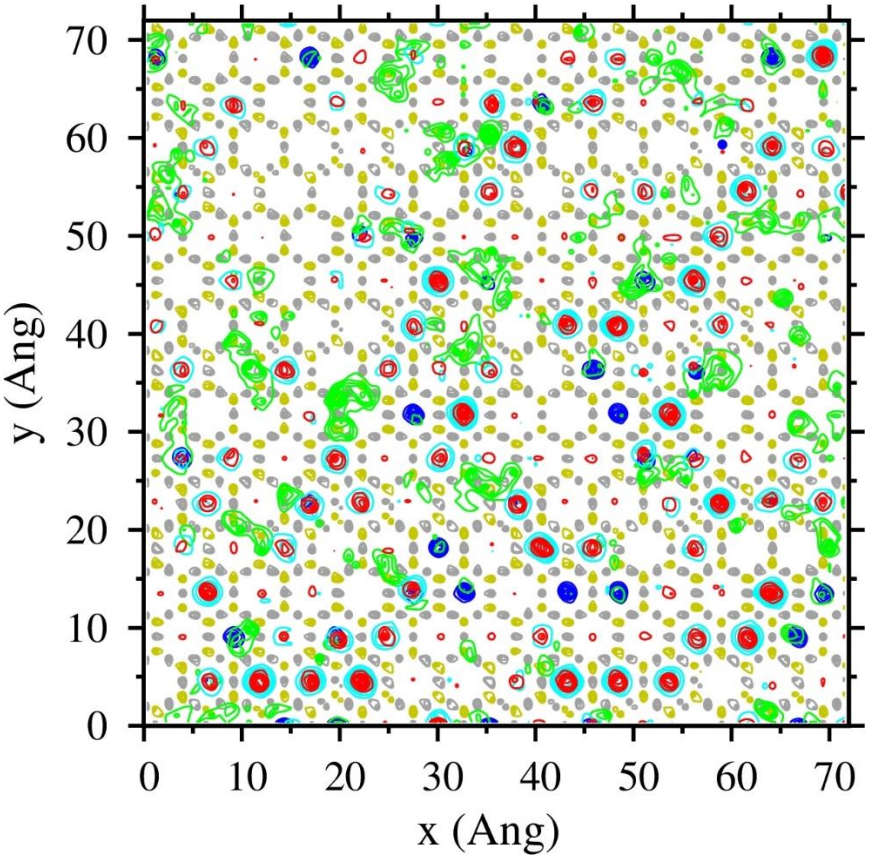

d)

Figure 6. Planar atomic density distributions (PADDs) of Cs^+ ions and O_{H2O} in the interlayers and on external surfaces of Cs-hectorite. a) Cs^+ ions and O_{H2O} atoms at distances $z < 3$ Å in the monolayer hydrate. b) schematic representation of the structural arrangement of H_2O (oxygen – red, hydrogen - cyan) molecules and Cs^+ ions (blue) in the monolayer hydrate. c) Cs^+ ions at distances $z < 2.8$ Å and O_{H2O} atoms at $z < 3.1$ Å in the bilayer hydrate. d) Cs^+ ions at $z < 2.8$ Å and O_{H2O} atoms at $z < 2.4$ Å on external basal surfaces. Color code: O_b – gray, Si – yellow, Cs^+ ions at the center of ditrigonal cavities – blue, Cs^+ ions above Si tetrahedron – green, O_{H2O} – red, H_{H2O} – cyan.

TABLES.

Hydration	***d (00l) Å***
Exp-dry[96]	10.665
Exp-dry [80]	11.700
Sim-dry (This work)	10.758
Exp-wet[80] (43%)	12.100
Exp-wet[81] (43%)	12.300
Sim-H_2O (This work)	12.426
Sim-H_2O[75,76]	12.410
Sim-H_2O[70]	12.420

Table 1. Interlayer spacings of dry and hydrated Cs-hectorites compared with previous experiments and simulation studies.

Hydration level	***H_2O diffusion ($10^{-9}m^2/s$)***
Mono-layer	0.179 ± 0.03
Bi-layer	1.152 ± 0.01
3 – layer	1.675 ± 0.05
External Surface	3.024 ± 0.02

Table 2. Diffusion coefficients of H_2O molecules in the interlayer galleries of the mono-, bi-, tri-layer hydrates and at the external basal surface of Cs-hectorite.

Hydration state	*Cs^+ - O_{H2O} (ps)*	*Cs^+ - O_b (ps)*	*O_{H2O} – O_b (ps)*
Intermittent (τ_{res}^I)			
Mono-layer	507	1038	326
Bi-layer	250	508	150
3 - layer	198	356	101
Continuous (τ_{res}^C)			
Mono-layer	28.5	62.5	6.5
Bi-layer	9.2	52.4	2.0
3 - layer	6.0	49.2	1.9

Table 3. Intermittent and continuous residence times for the indicated pairs in the interlayers of Cs-hectorite. Values are in ps.
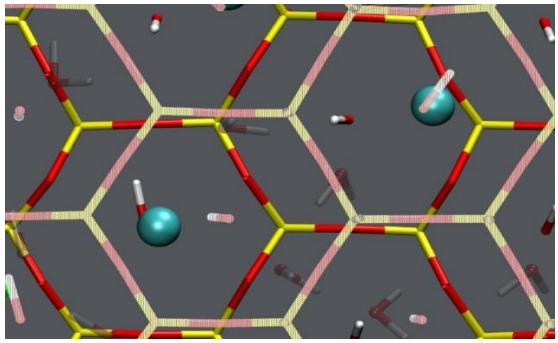
TOC Graphics